Transport Coefficients of the Anderson Model via the numerical renormalization group

T. A. Costi[1], A. C. Hewson[1] and V. Zlatić[2]

[1] Department of Mathematics, Imperial College, London SW7 2BZ, UK
[2] Institute of Physics, University of Zagreb, Croatia

Abstract. The transport coefficients of the Anderson model are calculated by extending Wilson's numerical renormalization group method to finite temperature Green's functions. Accurate results for the frequency and temperature dependence of the single–particle spectral densities and transport time $\tau(\omega, T)$ are obtained and used to extract the temperature dependence of the transport coefficients in the strong correlation limit of the Anderson model. Results are obtained for values of the local level position ranging from the Kondo regime to the mixed valency and empty orbital regimes. The low temperature anomalies in the resistivity, $\rho(T)$, thermopower, $S(T)$, thermal conductivity $\kappa(T)$ and Hall coefficient, $R_H(T)$, are discussed in terms of the behaviour of the spectral densities. All quantities exhibit the expected Fermi liquid behaviour at low temperature, $\rho(T) = \rho_0(1 - c(T/T_{\rm K})^2)$, $S(T) \sim \gamma T$, $\kappa(T)/\alpha\ T = 1 + \beta(T/T_{\rm K})^2$, $R_H(T) = -R_\infty(1 - \delta(T/T_{\rm K})^2)$. Analytic results based on Fermi liquid theory are derived here for the first time for β and the numerical results are shown to be consistent with this coefficient. The range of temperatures over which universal behaviour extends is also discussed. Scattering of conduction electrons in higher, $l > 0$, angular momentum channels is also considered and an expression is derived for the corresponding transport time and used to discuss the influence of the interference terms between the resonant $l = 0$ and non–resonant $l = 1$ channels on the transport properties. The presence of non–resonant scattering is shown to be particularly important for the thermopower at half–filling, where the sign of the thermopower can depend sensitively on the non–resonant phase shift. Finally the relation of the results to experiment is discussed.

Introduction

In this paper we present accurate results for the transport coefficients of the Anderson model obtained by extending the numerical renormalization group method [1, 2] to the calculation of finite temperature Green's functions. The Anderson model has been used extensively to interpret the properties of dilute magnetic alloys and a number of the local properties of heavy fermion compounds. It is also of use in discussing the properties of concentrated Kondo systems in cases where alloying or disorder inhibit the coherence effects between the magnetic ions. Although many of the properties of this model are now well understood [3], the temperature dependence of the transport coefficients has proved to be particularly difficult to calculate reliably. The transport coefficients require accurate expressions for both the temperature and frequency dependence of the impurity Green's function, a quantity which is difficult to calculate in the strong correlation limit of the Anderson model. Here we calculate this quantity from Wilson's numerical renormalization group method [1] which is non–perturbative and is therefore accurate for arbitrarily large Coulomb interactions. This method has played a crucial role in forming our current understanding of the Anderson model. It was first applied to the Kondo model by Wilson [1] and subsequently to the Anderson model by Krishnamurthy et al [2]. The two models are related via the Schrieffer–Wolff transformation [4], with the Kondo model describing the low–energy physics of the Anderson model in the strong correlation Kondo regime. The application of the numerical renormalization group to these models yielded the elementary excitations, thermodynamics, fixed points and effective Hamiltonians around the fixed points [1, 2]. Dynamic and transport properties were not calculated. The calculations showed that the Kondo model has two fixed points which characterize its physical properties. The local moment fixed point which describes the high temperature regime and in which the conduction electrons couple weakly to the impurity moment and a strong coupling fixed point which describes the low temperature regime in which the impurity moment is quenched and the excitations are those of a local Fermi liquid. The parameter space of the Anderson model is larger and the calculations showed that in addition to the local moment and strong coupling fixed points there are two additional fixed points. The most important of these is the valence fluctuation fixed point and is characteristic of the asymmetric model. In the valence fluctuation regime, charge fluctuations become important and the properties correspond to a model with a strongly renormalized temperature dependent resonant level [2]. In this paper we describe the transport coefficients and their relation to the corresponding spectral densities in these different regimes, pointing out the characteristic features which arise in each case.

In contrast to thermodynamic properties, which have been obtained exactly by the Bethe Ansatz [5, 6] and numerical renormalization group [1, 2], the calculation of transport and dynamic properties have relied on approximate methods. Finite order perturbation in U calculations give accurate results in the Fermi liquid regime for spectral densities and thermodynamic properties up to $U/\pi\Delta \approx 2.5$, where U is the

local Coulomb repulsion and Δ is the resonant level width in the Anderson model [7, 8]. However, in the local moment regime $U \gg \Delta$ for $T \gg T_{\rm K}$ where properties depend on logarithmic terms this approach breaks down. Quantum Monte Carlo approaches [10, 11] become increasingly less accurate for larger values of U and lower temperatures. So far transport coefficients via this method have been calculated for just the symmetric Anderson model and for $U/\pi\Delta \leq 3$ [12]. Transport coefficients have also been obtained for larger degeneracies of the local level N via the non–crossing approximation [13, 14]. A problem with this method is that it fails to satisfy the Fermi liquid relations at zero temperature [15]. In a finite magnetic field the transport coefficients for the Kondo model were discussed in [16] on the basis of the Nagaoka integral equations. Recently a comprehensive and highly accurate approach to the calculation of dynamic properties of magnetic impurity models has been developed by extending the numerical renormalization group approach [17, 18, 19, 20, 21, 22, 23]. This overcomes the above mentioned difficulties with the approximate methods. Accurate results in all regimes have been obtained for single–particle spectral densities at both zero [18, 19, 20, 21, 22] and finite temperature [23, 24]. These satisfy all the sum rules and Fermi liquid relations. In the next section we introduce the Anderson model including terms which model the scattering of conduction electrons in higher ($l > 0$) angular momentum channels. The transport coefficients are defined in terms of the transport time for conduction electrons scattering in both the the resonant and non–resonant channels (the transport time incorporating non–resonant scattering of conduction electrons is derived in Appendix A). The numerical renormalization group and its use in extracting finite temperature Greens's functions and spectral densities is then described. We also give analytic calculations for the low temperature behaviour of the transport coefficients based on Fermi liquid theory. These are used as a check on the accuracy of the numerical results. Finally we present the conclusions and indicate the relevance of the results to experiment.

Model, Transport Properties and Method

The model

The Anderson model including non–resonant scattering of conduction electrons in $l > 0$ channels is given by the following Hamiltonian

$$
\begin{aligned}
H &= H_{\rm imp} + H_{\rm hyb} + H_{\rm c}, \qquad (1)\\
H_{\rm imp} &= \sum_{\sigma} \epsilon_0 c^{\dagger}_{0\sigma} c_{0\sigma} + U n_{0\uparrow} n_{0\downarrow} + \sum_{l>0} \sum_{m=-l}^{+l} \epsilon_l c^{\dagger}_{lm} c_{lm},\\
H_{\rm hyb} &= \sum_{k\sigma} (V_{0k} c^{\dagger}_{k\sigma} c_{0\sigma} + H.c.) + \sum_{k\sigma\ l>0} \sum_{m=-l}^{+l} (V_{lmk} c^{\dagger}_{k\sigma} c_{lm} + H.c.),\\
H_{\rm c} &= \sum_{k\sigma} \epsilon_k c^{\dagger}_{k\sigma} c_{k\sigma}.
\end{aligned}
$$

The first term $H_{\rm imp}$ represents the impurity and is coupled to the conduction electrons $H_{\rm c}$ via the hybridization term $H_{\rm hyb}$. The scattering of conduction electrons in $l > 0$ channels is modelled by including uncorrelated levels, ϵ_l, hybridizing with the conduction electrons. This is equivalent to taking into account phase shifts η_l with $l > 0$ for the conduction electrons in addition to the usual $l = 0$ resonant phase shift. The charge neutrality condition requires that these phase shifts satisfy the Friedel sum rule [9]

$$Z = \sum_{l=0} 2(2l+1)\frac{\eta_l}{\pi}, \tag{2}$$

where Z is the excess charge on the impurity.

The many body effects arise from the strong Coulomb repulsion between the electrons in the impurity $l = 0$ level.

Transport coefficients

Assuming that the conduction electrons scatter incoherently from a small concentration, $n_i \ll 1$, of magnetic impurities, linear response theory allows the transport coefficients to be expressed in terms of the transport integrals [28]

$$L_{ml} = \int_{-\infty}^{+\infty} \left(-\frac{\partial f(\omega)}{\partial \omega}\right) \tau^l(\omega)(\omega-\mu)^m d\omega, \tag{3}$$

where μ is the chemical potential, and $\tau(\omega, T)$ is the transport time. The resistivity, $\rho(T)$, thermoelectric power, $S(T)$, thermal conductivity $\kappa(T)$ and Hall coefficient $R_H(T)$ are given in terms of these by

$$\rho(T) = \frac{1}{e^2 L_{01}} = \frac{1}{e^2} \frac{1}{\int \tau(\omega,T)\left(-\frac{\partial f}{\partial \omega}\right)\, d\omega}, \tag{4}$$

$$S(T) = -\frac{1}{|e|T}\frac{L_{11}}{L_{01}} = -\frac{1}{|e|T}\frac{\int \omega\tau(\omega,T)\left(-\frac{\partial f}{\partial \omega}\right)\, d\omega}{\int \tau(\omega,T)\left(-\frac{\partial f}{\partial \omega}\right)\, d\omega}, \tag{5}$$

$$\kappa(T) = \frac{1}{T}\left\{L_{21} - \frac{L_{11}^2}{L_{01}}\right\}, \tag{6}$$

$$R_H(T) = -R_\infty \frac{L_{02}}{L_{01}^2}, \tag{7}$$

where $R_\infty^{-1} = n_i|e|c$. In the absence of non–resonant scattering, the transport time, τ_0, (see Appendix A for constant factors such as n_i) is given by

$$\frac{1}{\tau_0(\omega,T)} = \Delta\rho_0(\omega,T), \tag{8}$$

where Δ is the resonant level width and ρ_0 is the single–particle spectral density. The latter is given in terms of the resonant level Green's function $G_0(\omega,T) = \langle\langle c_{0\sigma}; c_{0\sigma}^\dagger\rangle\rangle$ and self–energy $\Sigma(\omega,T) = \Sigma^R + i\Sigma^I$ by

$$\rho_0(\omega,T) = -\frac{1}{\pi} Im\, G_0(\omega,T) = \frac{1}{\pi}\frac{(\Delta - \Sigma^I(\omega))}{((\omega - \epsilon_0 - \Sigma^R(\omega))^2 + (\Delta - \Sigma^I(\omega))^2)}. \tag{9}$$

The transport time in the presence of non–resonant scattering is derived from the Kubo formula for the conductivity in Appendix A. In contrast to the case of resonant scattering only (see e.g. [13]), the vertex corrections for the current–current correlation functions entering the expressions for the transport coefficients are finite when non–resonant scattering is included. The resulting expression for the transport time after inclusion of vertex corrections is

$$\frac{1}{\tau(\omega,T)} = \frac{1}{\tau_0(\omega,T)}\left[\cos 2\eta_1 - \frac{Re\ G_0(\omega,T)}{Im\ G_0(\omega,T)}\sin 2\eta_1\right] + \rho_n. \tag{10}$$

The effects of non–resonant scattering are primarily contained in the factor $\left[\cos 2\eta_1 - \frac{Re\ G_0(\omega,T)}{Im\ G_0(\omega,T)}\sin 2\eta_1\right]$ which is due to interference between the $l = 0$ and $l = 1$ channels. The non–resonant, $l \neq 0$, phase–shifts in (10) are taken to be constants, defined by the screening charge in respective channels. Thus,

$$\rho_n = \frac{4\pi}{mk_{\rm F}}\left[\sin^2\eta_1 + \sum_{l>1} l\,\sin^2(\eta_l - \eta_{l-1})\right]. \tag{11}$$

In the $T = 0$ limit (but with $l \neq 0$) the transport coefficients calculated with (5) – (11) reduce to standard phase–shift expressions, while in the limit $\eta_{l\neq 0} \longrightarrow 0$ we recover the usual many–body expression for the single–channel transport time (8).

From the expressions for $\tau(\omega,T)$ and $\tau_0(\omega,T)$ we see that in order to evaluate the transport coefficients we require an accurate expression for the frequency and temperature dependent resonant Green's function $G_0(\omega,T)$. We obtain this from the numerical renormalization group method as described below.

The numerical renormalization group method

The numerical renormalization group for the Kondo and Anderson impurity models is described in [1, 2], where it was used to obtain the thermodynamic properties. Here we give a description of the method and its use in calculating finite temperature Green's functions and specifically the local Green's function $G_0(\omega,T)$ required for the transport time. The central idea in the numerical renormalization group is the importance of including all energy or length scales. The Hamiltonian (1) contains conduction electron states of all energies from the band edge D down to zero energy and states from each energy scale contribute to the impurity properties. To take into account these states Wilson introduced a logarithmic discretization of the conduction band about the Fermi level so that all energy scales were represented, with the greatest resolution at low energies where the many body effects are most important. As shown in Appendix B this logarithmic discretization approximation results in the following discrete Anderson model for the resonant channel,

$$\begin{aligned} H &= \lim_{N\to\infty}\frac{1}{2}(1+\Lambda^{-1})\Lambda^{-(N-1)/2}H_N, \\ H_N &= \Lambda^{(N-1)/2}[H_0 + H_{\rm hyb} + \sum_{n=0}^{N-1}\Lambda^{-n/2}\xi_n(f^\dagger_{n+1\sigma}f_{n\sigma} + f^\dagger_{n\sigma}f_{n+1\sigma})], \end{aligned} \tag{12}$$

where $H_0 = \epsilon_0 c^\dagger_{0\sigma} c_{0\sigma} + U n_{0\uparrow} n_{0\downarrow}$ is the resonant part of the impurity, $H_{\rm hyb} = V_0(f^\dagger_{0\sigma} c_{0\sigma} + H.c.)$ couples the impurity to a local conduction electron orbital $f^\dagger_{0\sigma}|0>$, and the last term describes the remaining conduction electron orbitals whose wavefunctions have a large overlap with the impurity. The conduction electron orbitals neglected in the above discrete approximation to the full Anderson model have their wavefunctions localized away from the impurity site and have negligible contributions to the impurity properties (see Appendix B and [2] for further details). The parameter $\Lambda > 1$ describes the discretization of the conduction band. The above discretized Hamiltonian is in the form of a semi–infinite linear chain and can be iteratively diagonalized for increasing chain lengths N to obtain the eigenvalues, E^N_p, and eigenvectors, $|p>_N$, on successively lower energy scales $\omega_N \approx D\Lambda^{-\frac{N-1}{2}}$, where ω_N is the lowest scale of H_N (see Appendix B for details). From the eigenvalues, the thermodynamic properties are obtained at a corresponding sequence of temperatures $T_N \approx \omega_N/k_B$. The details are given in [2] and in Appendix B. Here we show how the local Green's functions can be extracted on successively lower energy scales.

Consider the Green's function $G_0(\omega, T) = \langle\langle c_{0\sigma}; c^\dagger_{0\sigma}\rangle\rangle$. Using H_N, the N'th shell Green's function $G^N_0(\omega, T)$ and associated spectral density $\rho^N_0(\omega, T)$ are given by

$$G^N_{0\sigma}(\omega, T) = \langle\langle c_{0\sigma}; c^\dagger_{0\sigma}\rangle\rangle = \frac{1}{Z_N(\beta)} \sum_{pp'} \frac{|M^N_{pp'}|^2 (e^{-\beta E^N_p} + e^{-\beta E^N_{p'}})}{\omega - E^N_{p'} + E^N_p}, \tag{13}$$

$$\rho^N_0(\omega, T) = \frac{1}{Z_N(\beta)} \sum_{pp'} |M^N_{pp'}|^2 (e^{-\beta E^N_p} + e^{-\beta E^N_{p'}}) \delta(\omega - E^N_{p'} + E^N_p). \tag{14}$$

Here $Z_N(\beta)$ is the partition function for the $N'th$ cluster, and $M^N_{pp'} = \langle p|c_{0\sigma}|p'\rangle$ are the many–body matrix elements of the local operator $c_{0\sigma}$. The latter can be evaluated recursively in a similar way to the evaluation of the matrix elements $\langle p|f_{N\sigma}|q\rangle$ in (B.14). Using the unitary transformation (B.13) we obtain

$$\begin{aligned} M^N_{pp'} &= \langle p|c_{0\sigma}|p'\rangle_N \\ &= \sum_{r,i} \sum_{r',i'} U^*_N(p, ri) U_N(q, r'i') \langle i|\langle r|c_{0\sigma}|r'\rangle|i'\rangle \\ &= \sum_{r,i} \sum_{r',i'} U^*_N(p, ri) U_N(q, r'i') \delta_{i,i'} M^{N-1}_{r,r'}. \end{aligned} \tag{15}$$

Hence the matrix elements $M^N_{pp'}$ can be evaluated recursively from a knowledge of the eigenstates of the N'th cluster, $U_N(p, ri)$, and the matrix elements, $M^{N-1}_{rr'}$, of the previous cluster. For a given cluster size N the Hamiltonian H_N only describes excitations in a limited range of width $K\omega_N$ above the lowest scale ω_N present in H_N, due to the truncation of the spectrum as described in Appendix B. At $T = 0$ the spectral density is evaluated at $\omega \approx 2\omega_N$. Calculating the spectral density at energies much smaller than this using H_N is not justified, since information on lower energies is obtained in subsequent iterations, whereas calculating the spectral densities at much higher energies than this might introduce errors due to the truncation of the spectrum

on the high energy side. In evaluating (14) the delta functions are broadened with Gaussians of width α_N of order ω_N appropriate to the cluster size. The broadening parameter α_N used within each energy shell is varied continuously so that there is no discontinuity in going between successive iterations. The small remaining asymmetry in the spectral features due to the larger broadening parameter at the higher excitations should vanish in the limit $\Lambda \to 1$. The procedure for calculating finite temperature Green's functions is slightly more complicated. The shell Green's function $G_0^N(\omega, T)$ and spectral density $\rho_0^N(\omega, T)$ are only reliable for excitations $\omega \approx 2\omega_N$ and for temperatures $k_B T \ll 2\omega_N$. For temperatures $k_B T \gg 2\omega_N$ excited states not contained in H_N would be important, whilst for temperatures $k_B T$ of order $2\omega_N$ transitions between *excited* states would need to be known accurately. In principle these are known from subsequent iterations, but are not contained with sufficient accuracy in H_N. The only transitions known with sufficient accuracy in H_N are the groundstate to excited state transitions with excitation energies $\approx 2\omega_N$ which is the natural energy scale of this *cluster*‡. As long as $k_B T \ll 2\omega_N$ it is not necessary to know the lower excitations since their contribution to the Green's function and spectral density *for the energies* $\omega = 2\omega_N$ *under consideration* will be negligible (note the delta function in (14)). From this discussion it follows that the spectral density for temperature T can be calculated from the shell spectral densities $\rho_0^i(\omega, T)$ at frequencies $\omega \approx 2\omega_i$ for $i = 1, 2, \ldots, M$ until $2\omega_M$ becomes of order T. To calculate the spectral density at temperature T and for frequencies below $2\omega_M$, a smaller cluster is used. This is done because when T is larger than the frequency at which the spectral density is being evaluated, it is the excited states of order T contained in previous clusters which are important and not the excitations very much below T. The procedure outlined here requires storing all the matrix elements for the Green's functions for each cluster size, since smaller clusters may be required in subsequent iterations.

In the absence of non–resonant scattering we can calculate the transport time $\tau_0(\omega, T)$ directly from the single–particle spectral density $\rho_0(\omega, T)$ using (8) and hence the transport coefficients (4–7). In the presence of non–resonant scattering, we evaluate in addition the real part of $G_0(\omega, T)$ and use (10) and (4–7) to calculate the transport coefficients. In the next section we present the numerical results obtained using this procedure.

Low temperature results

Before presenting numerical results we outline some analytic results on the low temperature behaviour of the transport coefficients obtained by using Fermi liquid theory. These serve as an independent check on the accuracy of the numerical renormalization group method. In the following analytic calculations we restrict ourselves to the case of resonant scattering only so the transport time $\tau(\omega, T) = \tau_0(\omega, T)$.

To extract the low temperature behaviour of the transport coefficients we use the

‡ The term cluster is suggested by the notation although the calculations are in k–space

Sommerfeld expansion. In the transport integrals (3) the factor $\left(-\frac{\partial f}{\partial \omega}\right)$ for temperature T provides an energy cut off outside the Fermi window $|\omega| < T$. The functional form of $G_0(\omega, T)$ also has an energy scale $|\omega| \ll k_{\rm B}T_0$ over which $\tau(\omega, T)$ is a a slowly varying function, where $T_0 = T_{\rm K}$ for the Kondo regime and $k_{\rm B}T_0 = \Delta$, for the mixed valency regime. As a consequence, for temperatures $T \ll T_0$, we can apply the Sommerfeld expansion,

$$\int_{-\infty}^{+\infty} \left(-\frac{\partial f}{\partial \omega}\right) h(\omega, T) d\omega = h(\epsilon_{\rm F}, T) + \frac{\pi^2}{6}(k_B T)^2 \left(\frac{\partial^2 h(\omega, T)}{\partial \omega^2}\right)_{\omega=\epsilon_{\rm F}} + \frac{7\pi^4}{720}(k_B T)^4 \left(\frac{\partial^4 h(\omega, T)}{\partial \omega^4}\right)_{\omega=\epsilon_{\rm F}} + O(T^6). \quad (16)$$

The quantity $h(\omega, T)$ entering the above expression is $\tau^l(\omega, T)\omega^m$ for the integral L_{ml}. For the Kondo problem the transport time $\tau(\omega, T)$ is a strong function of temperature at the Fermi level, so in the Sommerfeld expansion in addition to the temperature dependence coming from the fermi function there is also the explicit temperature dependence of the transport time at the Fermi level. This is taken into account by expanding $\tau(\epsilon_{\rm F}, T)$ in a Taylor series

$$\tau(\epsilon_{\rm F}, T) = \tau(\epsilon_{\rm F}, 0) + \frac{1}{2}T^2 \left(\frac{\partial^2 \tau(\epsilon_{\rm F}, T)}{\partial T^2}\right)_{T=0} + O(T^4) \quad (17)$$

In the Sommerfeld expansions for the resistivity, thermopower, thermal conductivity and Hall coefficient the derivatives which enter are $\frac{1}{\tau}\frac{\partial \tau}{\partial \omega}$, $\frac{1}{\tau}\frac{\partial^2 \tau}{\partial \omega^2}$, and $\frac{1}{\tau}\frac{\partial^2 \tau}{\partial T^2}$. Since $\tau_0(\omega, T) = 1/\Delta\rho_0(\omega, T)$ these derivatives are given by

$$\frac{1}{\tau}\frac{\partial \tau}{\partial \omega} = -\frac{1}{\rho_0}\frac{\partial \rho_0}{\partial \omega}, \quad (18)$$

$$\frac{1}{\tau}\frac{\partial^2 \tau}{\partial \omega^2} = 2\left(\frac{1}{\rho_0}\frac{\partial \rho_0}{\partial \omega}\right)^2 - \left(\frac{1}{\rho_0}\frac{\partial^2 \rho_0}{\partial \omega^2}\right), \quad (19)$$

$$\frac{1}{\tau}\frac{\partial^2 \tau}{\partial T^2} = -\left(\frac{1}{\rho_0}\frac{\partial^2 \rho_0}{\partial T^2}.\right) \quad (20)$$

Using (9) we obtain for the energy derivatives at $\omega = \epsilon_{\rm F}$ and $T = 0$,

$$\frac{1}{\rho_0}\left(\frac{\partial \rho_0}{\partial \omega}\right) = 3\gamma \cot(\pi n_0/2), \quad (21)$$

$$\left(\frac{1}{\rho_0}\frac{\partial^2 \rho_0}{\partial \omega^2}\right) = -\frac{1}{\Delta}\left(\frac{\partial^2 \Sigma^I}{\partial \omega^2}\right) + \left(\frac{2\pi\rho_0(\epsilon_{\rm F}, 0)}{z}\right)^2 \cot^2(\pi n_0/2) + 2\pi\Delta\rho_0(\epsilon_{\rm F}, 0)\left(-\frac{1}{\tilde{\Delta}^2} + \frac{1}{\Delta}\left(\frac{\partial^2 \Sigma^I}{\partial \omega^2}\right) - \frac{\cot(\pi n_0/2)}{\Delta}\left(\frac{\partial^2 \Sigma^R}{\partial \omega^2}\right)\right), \quad (22)$$

where $\tilde{\Delta} = z\Delta$ and $z = (1 - \frac{\partial \Sigma^R}{\partial \omega})^{-1}_{\omega=\epsilon_{\rm F}}$ is the wavefunction renormalization constant. In deriving the above we have used (9) and the Fermi liquid properties of the self–energy $\Sigma^R(\omega, 0) \sim \omega$ and $\Sigma^I(\omega, 0) \sim (\omega - \epsilon_{\rm F})^2$. The quantity n_0 is the local level occupancy

and γ is the linear coefficient of the low temperature specific heat. The latter is given by [3]

$$\gamma = \frac{2}{3}\pi k_B^2 \frac{\tilde{\Delta}}{\tilde{\epsilon_0^2} + \tilde{\Delta}^2}, \tag{23}$$

where $\tilde{\epsilon_0} = z(\epsilon_0 + \Sigma^R(\epsilon_{\rm F}, 0))$. In the Kondo regime $z \ll 1$ and $\tilde{\Delta} \sim k_{\rm B}T_{\rm K} \ll \Delta$ which leads to a large enhancement of γ since from (23) $\gamma \sim 1/T_{\rm K}$. The Kondo temperature, $T_{\rm K}$, is given by [29]

$$k_B T_{\rm K} = U\left(\frac{\Delta}{2U}\right)^{1/2} e^{\pi\epsilon_0(\epsilon_0+U)/2\Delta U} \tag{24}$$

For the thermopower we require only the first energy derivative of ρ_0 to extract the leading term. We have from (5) and (16),

$$S(T) = -\frac{1}{|e|T}\frac{\frac{\pi^2}{6}(k_BT)^2\left[\frac{\partial^2[\omega\tau(\omega)]}{\partial\omega^2}\right]_{\omega=\epsilon_{\rm F}} + O(T^4)}{\tau(\epsilon_{\rm F})\left[1 + \frac{\pi^2}{6}(k_BT)^2\frac{1}{\tau(\epsilon_{\rm F})}\left[\frac{\partial^2\tau(\omega)}{\partial\omega^2}\right]_{\omega=\epsilon_{\rm F}}\right] + O(T^4)} \tag{25}$$

which on using (18,21) reduces to the Fermi liquid result, [33, 35]

$$S(T) = \frac{\pi\gamma T}{|e|}\cot(\pi n_0/2) + O(T^3), \tag{26}$$

and can be checked by evaluating S, γ and n_0 within the numerical renormalization group technique [24].

To extract the other transport coefficients to lowest order in T requires the second derivative with respect temperature of τ_0 and hence an expression for the self–energy correct to order T^2. This is difficult to obtain analytically in the general case so we restrict ourselves to just the symmetric case. The self–energy for the symmetric model correct to order ω^2 and T^2 is given by [31, 32]

$$\Sigma(\omega,T) = \Sigma^R(\omega,T) + i\Sigma^I(\omega,T) = \Sigma^R(\omega,0) - i\frac{\Gamma_0^2}{2\Delta(\pi\Delta)^2}(\omega^2 + \pi^2(k_BT)^2), \tag{27}$$

where Γ_0 is the irreducible vertex function evaluated at zero frequency [31, 32]. Using (27) we obtain the temperature derivative,

$$\left(\frac{1}{\tau}\frac{\partial^2\tau}{\partial T^2}\right)_{\omega=\epsilon_{\rm F},T=0} = -\left(\frac{1}{\rho_0}\frac{\partial^2\rho_0}{\partial T^2}\right) = \frac{k_B^2\Gamma_0^2}{\pi\Delta}\frac{1}{((\epsilon_0+\Sigma^R)^2+\Delta^2)^2}. \tag{28}$$

We now use these results to first check the exact result for the T^2 coefficient of the resistivity first derived by Nozières [30] and Yamada [31, 32] and then derive the exact coefficient for the T^2 coefficient of $(\kappa(T)/T)/(\kappa(T)/T)_{T\to 0}$. Restricting the discussion to the Kondo regime where the charge susceptibility is zero so $\Gamma_0 = \pi\Delta/z$, and the particle-hole symmetric model where $\epsilon_0 + \Sigma^R = 0$, we find from (22, 28)

$$\left(\frac{1}{\tau}\frac{\partial^2\tau}{\partial\omega^2}\right)_{\omega=\epsilon_{\rm F},T=0} = 3/\tilde{\Delta}^2, \text{ and } \left(\frac{1}{\tau}\frac{\partial^2\tau}{\partial T^2}\right)_{\omega=\epsilon_{\rm F},T=0} = \pi^2k_B^2/\tilde{\Delta}^2. \tag{29}$$

Hence from (4,16,17) and (29) we have for the resistivity,

$$\begin{aligned}\rho(T) &= \frac{1}{e^2\tau(\epsilon_{\rm F},0)\left[1+\frac{1}{2}T^2\frac{1}{\tau(\epsilon_{\rm F},0)}\frac{\partial^2\tau}{\partial T^2}+\frac{\pi^2(k_BT)^2}{6}\frac{1}{\tau(\epsilon_{\rm F},0)}\frac{\partial^2\tau}{\partial\omega^2}+O(T^4)\right]},\\ &= \frac{1}{e^2\tau(\epsilon_{\rm F},0)\left[1+\frac{1}{2}\frac{\pi^2k_B^2}{\tilde{\Delta}^2}T^2+\frac{1}{2}\frac{\pi^2k_B^2}{\tilde{\Delta}^2}T^2+O(T^4)\right]},\\ &= \rho(0)(1-c\left(\frac{T}{T_{\rm K}}\right)^2), \end{aligned} \tag{30}$$

where $\rho(0)=1/e^2\tau(\epsilon_{\rm F},0)$ and $c=\pi^2k_B^2T_{\rm K}^2/\tilde{\Delta}^2=\pi^4/16=6.088$ and we have used the result for the symmetric case $\pi\tilde{\Delta}=4k_BT_{\rm K}$ [31, 32]. The above result for c is the exact result obtained by Nozières [30]. Without the contribution from (28) the coefficient c would have been wrong by a factor of 2. Away from the symmetric case the result of Nozières will be modified due terms in (18–19) which depend on the occupation number n_0 and also due to additional temperature dependences coming from the occupation number and the imaginary part of the self–energy. These are difficult to estimate analytically, but our numerical results to be presented in the next section give some indication of their size. Most terms depend on $\cot(\pi n_0/2)$ and are expected to be small in the Kondo regime $n_0\approx 1$.

We now prove an exact Fermi liquid result for the thermal conductivity. Using $|e|S(T)/T=\pi\gamma\cot(\pi n_0/2)$ we have

$$\frac{\kappa(T)}{T}=\frac{1}{T^2}L_{21}+\pi\gamma\cot(\pi n_0/2)L_{11}. \tag{31}$$

The expansion for L_{21} is

$$\begin{aligned}L_{21} &= \int_{-\infty}^{+\infty}\left(-\frac{\partial f}{\partial\omega}\right)\omega^2\tau(\omega,T)d\omega,\\ &= \frac{\pi^2}{6}(k_BT)^2\left(\frac{\partial^2(\omega^2\tau(\omega))}{\partial\omega^2}\right)_{\omega=\epsilon_{\rm F}}+\frac{7\pi^4}{720}(k_BT)^4\left(\frac{\partial^4(\omega^2\tau(\omega))}{\partial\omega^4}\right)_{\omega=\epsilon_{\rm F}}+O(T^6),\\ &= \frac{\pi^2k_B^2T^2}{3}\tau(\epsilon_{\rm F},0)\left[1+\frac{3}{2\pi^2k_B^2}T^2\frac{1}{\tau}\left(\frac{\partial^2\tau}{\partial T^2}\right)_{T=0}\right]+\frac{7\pi^4}{60}(k_BT)^4\left(\frac{\partial^2\tau}{\partial\omega^2}\right)_{\omega=\epsilon_{\rm F}}+O(T^6),\\ &= \frac{\pi^2k_B^2T^2}{3}\tau(\epsilon_{\rm F},0)\left[1+\frac{3}{2\pi^2k_B^2}T^2\frac{1}{\tau}\left(\frac{\partial^2\tau}{\partial T^2}\right)_{T=0}+\frac{7\pi^2k_B^2T^2}{20}\frac{1}{\tau}\left(\frac{\partial^2\tau}{\partial\omega^2}\right)_{\omega=\epsilon_{\rm F}}+O(T^4)\right]. \end{aligned} \tag{32}$$

Substituting this into the expression for the thermal conductivity, and using the above results for the derivatives we obtain for the symmetric case in the Kondo limit,

$$\frac{\kappa(T)}{T}/(\frac{\kappa(T)}{T})_0=1+\beta\left(\frac{T}{T_{\rm K}}\right)^2, \tag{33}$$

where $\beta=26c/10=13\pi^4/80=15.83$ and the linear coefficient of κ is $\alpha=\left(\frac{\kappa(T)}{T}\right)_0=\pi^2k_B^2\tau(\epsilon_{\rm F},0)/3$. In the asymmetric case there will be additional contributions to the thermal conductivity which will modify the coefficient β. As discussed earlier for the

resistivity these will be difficult to estimate but are expected to be small in the Kondo regime, so we expect the coefficient β to remain close to its symmetric value $13\pi^4/80$.

The low temperature behaviour of the Hall coefficient can also be extracted. From the Sommerfeld expansion it can be shown that the order T^2 terms from the energy derivatives cancel and that the T^2 term results from the temperature dependence of τ at the Fermi level, yielding in the symmetric case $R_H(T) \sim -R_\infty(1 - \delta(T/T_{\rm K})^2)$ where the coefficient δ depends on second derivatives and a fourth derivative $(\partial^4\tau/\partial\omega^2\partial T^2)_{\omega=\epsilon_{\rm F},T=0}$. We do not evaluate this since as discussed in the section on numerical results, there is a much larger contribution to the Hall effect due to skew scattering of electrons which should be included for a discussion of the Hall coefficient of magnetic impurities [39, 40].

To summarize the analytic calculations, we see that in Fermi liquid theory in the Kondo regime that the transport coefficients all scale with $T_{\rm K}$ at low temperature. Specifically we have

$$\rho(T) = \rho(0)(1 - c\,(T/T_{\rm K})^2), \tag{34}$$

$$S(T) = \frac{\pi\gamma T}{|e|}\cot(\eta_0(\epsilon_{\rm F})) \sim (T/T_{\rm K}), \tag{35}$$

$$(\kappa(T)/T)\,/\,(\kappa(T)/T)_0 = 1 + \beta(T/T_{\rm K})^2, \tag{36}$$

$$R_H(T)/R_\infty = -(1 - \delta(T/T_{\rm K})^2), \tag{37}$$

where the constants c, α, β, γ and δ depend on τ and its derivatives at the Fermi level. For the symmetric model one finds,

$$c = \frac{\pi^4}{16} = 6.088, \tag{38}$$

$$\alpha = (\frac{\kappa(T)}{T})_0 = \frac{k_B^2\pi^2}{3}\tau(\epsilon_{\rm F}, 0), \tag{39}$$

$$\beta = (13/80)\pi^4 = 15.83, \tag{40}$$

$$\gamma = \frac{\pi^2}{6k_BT_{\rm K}}. \tag{41}$$

Corresponding expression for arbitrary U can be derived from a renormalized perturbation theory in terms of $\tilde{\Delta}$ and a renormalized interaction $\tilde{U} = z^2\Gamma_0$ [37].

In the asymmetric case for the Kondo regime $n_0 \approx 1$, there should be negligible corrections to these coefficients, the asymmetry in this regime should only affect the value of $T_{\rm K}$.

The functional form of the low temperature transport coefficients in the Kondo regime (34–37) and the coefficients of the leading order terms (38–41) in the symmetric case provide a check on the accuracy of the numerical renormalization group results presented in the next section.

Numerical results

The numerical results presented here are for the strong correlation limit of the Anderson model, i.e. $U/\pi\Delta \gg 1$. We take $U/\pi\Delta = 4$, unless otherwise indicated. The local level position takes values $\epsilon_0/\Delta = -U/2\Delta = -2\pi$ corresponding to the symmetric case and $\epsilon_0/\Delta = -4, -3, -2, -1, 0, +1$ corresponding to the asymmetric case. We are mainly interested in universal effects independent of the band structure, so all parameters are small relative to the conduction electron half–bandwidth $D = 1$. Specifically we used $\Delta = 0.01D$. For $\epsilon_0/\Delta = -4, -3, -2$ the parameters describe the Kondo regime, whilst for $\epsilon_0/\Delta = -1, 0$ and $\epsilon_0/\Delta = +1$ they describe mixed valency and empty orbital regimes respectively. In discussing the effects of non–resonant scattering on the transport properties we took a small $l = 1$ phase shift, $\eta_1 = \pm 0.01\pi, \pm 0.02\pi, \ldots, \pm 0.05\pi$. The discretization parameter Λ can be taken as low as 1.5 without encountering large errors due to the truncation of high energy states. The use of such a small value of Λ does introduce errors into the spectral densities for extremely low energies. These are noticeable in the symmetric case for example, where for sufficiently low energies $\omega \ll k_B T_{\rm K}$, the symmetry of the spectral density is violated slightly. A larger value of Λ allowing the lower energies to be reached in fewer iterations could be used to avoid this problem, however this was not necessary in the present calculations.

Thermodynamics

The thermodynamic properties of the Anderson model have been discussed in [2] where the static susceptibility was calculated over the whole temperature range from the band edge down to temperatures $T \ll T_{\rm K}$. The specific heat was calculated in the strong coupling regime $T \ll T_{\rm K}$ by perturbation theory on the effective Hamiltonian around the strong coupling fixed point [2]. Here we briefly present the results for the local level occupancy $n_0(T)$ and specific heat $C(T)$ over the whole temperature regime of interest (calculations of $C(T)$ for the screened Anderson model where presented in [21]).

Local level occupancy, $n_0(T)$ The local level occupancy $n_0(T)$ can be calculated at a sequence of temperatures $T_N, N = 1, 2, \ldots$ from the average electron number on the impurity and is shown in Fig. 1 for several values of the local level position ranging from the Kondo regime ($\epsilon_0/\Delta = -4, -3, -2$) to the mixed valency ($\epsilon_0/\Delta = -1, 0$) and empty orbital regime ($\epsilon_0/\Delta = +1$). The only significant temperature variation occurs on the valence fluctuation temperature scale $k_B T = \Delta = 10^{-2} D$. On the Kondo temperture scale, $T_{\rm K}$ (listed in Table 1), the variation of n_0 is insignificant indicating that the Kondo resonance has negligible weight in agreement with the spectral densities presented below. The values of $n_0(T = 0)$ are shown in Table 1.

Specific heat The specific heat, shown in Fig. 2, exhibits one or two distinct peaks depending on the position of the local level. In the Kondo regime there are two distinct

Table 1. The first column shows the local level positions used in the calculations, and the other columns show various data extracted. $\rho_0^{\rm Friedel} = \frac{\sin^2(\pi n_0/2)}{\pi\Delta}$, where n_0 is the local level occupancy at $T = 0$ and is extracted from the partition function. The T^2 coefficient of the resistivity in the Kondo regime is defined by $c = \lim_{T\to 0}\left(\frac{1-\rho(T)/\rho(0)}{(T/T_{\rm K})^2}\right)$, which according to Fermi liquid theory should be 6.088 in the symmetric case with small corrections in the asymmetric Kondo regime. The linear coefficient of the thermal conductivity is $\alpha = \left(\frac{\kappa(T)}{T}\right)_{T\to 0}$ and β is the T^2 coefficient of $\kappa(T)/\alpha T$ which should be 15.83 in the symmetric case.

ϵ_0	n_0	γ/k_B^2	$T_{\rm K}/\Delta$	$\rho_0^{Friedel}$	$\rho_0^{NRG}(\epsilon_{\rm F},0)$	% error	c	% error	α	β
$\epsilon_0 = -\frac{U}{2}$	1.00	8055.5	0.0180	31.83	32.61	-2.4%	5.7	-6.4%	0.102	11.6
$\epsilon_0 = -4\Delta$	0.93	4224.0	0.0346	31.45	32.13	-2.1%	5.8	-4.7%	0.101	13.5
$\epsilon_0 = -3\Delta$	0.88	2069.0	0.0690	31.26	31.33	-0.2%	6.4	+5.1%	0.106	12.6
$\epsilon_0 = -2\Delta$	0.78	832.0	0.1790	28.34	28.93	-2.0%	6.6	+8.4%	0.113	13.2
$\epsilon_0 = -\Delta$	0.63	281.0	0.5900	22.14	22.32	-0.8%	—	—	0.147	—
$\epsilon_0 = 0$ —	0.45	100.7	2.5100	13.18	13.36	-1.4%	—	—	0.246	—
$\epsilon_0 = +\Delta$	0.31	42.2	13.660	6.85	6.79	+0.9%	—	—	0.496	—

peaks, one at $T \approx T_{\rm K}$ and another at T of the order of Δ. The low energy peak, which is observed in many systems, is associated with the entropy of the magnetic impurity so the area under this peak is given by $k_B \ln(2)$ for the present case where the impurity has $S = 1/2$. The higher peak is associated with the charge degrees of freedom. The same behaviour is found in the Bethe–Ansatz solution [34]. In Fig. 3 we show the ratio $C(T)/T$. The linear in T behaviour characteristic of a Fermi liquid is clear and we tabulate the linear coefficient in Table 1. Finally, Fig. 4 shows that the specific heat is a universal function of $T/T_{\rm K}$ in the Kondo regime. Universality for this quantity extends up to $T \approx 5T_{\rm K}$ for the case $\epsilon_0/\Delta = -4$. From the figure it seems very likely that in the Kondo regime and provided the local level is very far from the Fermi level the universal behaviour should extend over the whole range $10T_{\rm K}$ of the low low energy peak.

In the mixed valency regime there is a peak slightly below the valence fluctuation temperature scale $k_B T = \Delta$ and a shoulder or small peak at higher temperatures. The same behaviour is found in the empty orbital case. The same behaviour is found also from the Bethe–Ansatz solution [34].

The value of the linear coefficient of specific heat has been checked in the case of $U = 0$ and found to be in good agreement with the exact result. It has also been checked independently for both $U = 0$ and finite U [38] by using the Fermi liquid relation,

$$\frac{4\chi_s}{(g\mu_B)^2} + \chi_c = \frac{6}{(k_B\pi)^2}\gamma, \tag{42}$$

where χ_s and χ_c are the spin and charge susceptibilities and can be obtained as thermodynamic quantities or from the corresponding dynamic susceptibilities. This Fermi liquid relation has been shown to be satisfied within a few percent and provides an independent test on the accuracy of γ from the present thermodynamic calculation

[38]

Spectral densities

The spectral densities in the Kondo regime are shown in Fig. 5–7 for zero and finite temperatures. At low temperatures $T \ll T_{\rm K}$ the spectral density is characterized by three resonances: the Kondo resonance at the Fermi level of width $T_{\rm K}$ and negligible weight and two atomic–like resonances on either side close to the bare excitation energies ϵ_0 and $\epsilon_0 + U$. The latter contain most of the spectral weight and have widths of order Δ. The Kondo resonance lies at the Fermi level in the symmetric case $\epsilon_0 = -U/2$ and above the Fermi level in the asymmetric case $\epsilon_0 > -U/2$ (see inset to Fig. 5). The width of the Kondo resonance is approximately $T_{\rm K}$, where $T_{\rm K}$ is defined in (24) and shows the correct exponential dependence on ϵ_0 and U (inset to Fig. 5 and [23]). On increasing the temperature, the Kondo resonance decreases rapidly in height and eventually disappears completely for $T \gg T_{\rm K}$ (Fig. 6–7). The atomic–like peaks remain temperature independent until $k_{\rm B}T \approx \Delta$. For $k_{\rm B}T \geq \Delta$ they acquire some temperature dependence, and in the asymmetric case, Fig. 7, there is a transfer of spectral weight from the lower to the upper peak with increasing temperature. In the symmetric case, Fig. 6, no spectral weight can be transferred but instead the two peaks broaden with increasing temperature. The positions of these high energy peaks changes little with temperature. Qualitatively similar results for the temperature dependence of the spectral densities have been obtained by perturbative methods for $U/\pi\Delta \leq 2.5$ [7]. The spectral densities in the mixed valency and empty orbital regimes are shown in Fig. 8–10 for zero and finite temperatures. In these regimes the spectral density at low temperatures, $k_B T \ll \Delta$, is characterized by two resonances (see Fig.8–10): one at $\tilde{\epsilon_0}$ of width approximately Δ and a much broader resonance at $\tilde{\epsilon_0} + U$ carrying very much less weight. In the mixed valency regime, $\epsilon_0/\Delta \approx -1$, the bare level is renormalized by the interactions to lie above the Fermi level $\tilde{\epsilon_0} > 0$. The bare level is also renormalized to higher energies in the empty orbital case , i.e. $\tilde{\epsilon_0} > \epsilon_0 \geq \Delta$. On increasing temperature, the main effect in the mixed valence case is a strong temperature dependence of the resonance at $\tilde{\epsilon_0}$ on a scale of order Δ (see Fig. 9–10). This resonance broadens and decreases in height with increasing temperature, but does not completely disappear at high temperature. In addition it always remains above the Fermi level. The resonance at $\tilde{\epsilon_0} + U$ remains distinct from that $\tilde{\epsilon_0}$ up to at least $k_{\rm B}T \approx 6\Delta$. Similar behaviour occurs in the empty orbital regime but the relevant energy scale for the temperature dependence in this case is set by $\tilde{\epsilon}_0$.

A good test on the accuracy of the spectral densities is provided by the Friedel sum rule which relates the spectral density at the Fermi level to the $T = 0$ occupation number $n_0(T = 0)$:

$$\rho_0(\omega = \epsilon_{\rm F}, T = 0) = \frac{1}{\pi\Delta} \sin^2(\pi n_0/2). \tag{43}$$

Using $n_0(T = 0)$ calculated from the partition function gives agreement to within 3% in all parameter regimes as shown in Table 1. The values of $n_0(T = 0)$ calculated from

the spectral densities are within 3% of those calculated from the partition function, but the former are expected to be essentially exact since they are obtained from the low energy part of the spectrum ($n_0(T=0) = \lim_{T_N \to 0} \langle n_0 \rangle_{T_N}$) where the method gives the highest resolution. It should be noted that the value of n_0 calculated from the spectral density is largely due to the high energy features at ϵ_0, where the method has less resolution due to the logarithmic discretization of the conduction band. However, the agreement to within 3% between the values of n_0 calculated by these two different ways provides additional evidence that method can give accurate results for high energy spectral features as well as low energy ones. The high energy features have a small asymmetry due the broadening procedure used for the delta functions in the spectral density which should vanish in the limit $\Lambda \to 1$ (as described earlier).

Transport coefficients

Resistivity Results for the resistivity are shown in Fig. 11 for several values of the local level position ranging from the Kondo regime ($\epsilon_0/\Delta = -\frac{U}{2\Delta}, -4, -3, -2$) to the mixed valency ($\epsilon_0/\Delta = -1, 0$) and empty orbital ($\epsilon_0/\Delta = +1$) regimes. The behaviour of the resistivity is qualitatively similar in all regimes with a monotonic increase with decreasing temperature. At $T = 0$ it reaches its limit $\rho(0) = 1/e^2\tau_0(\epsilon_{\rm F}, 0)$. Since $\tau_0 \sim 1/\rho_0$ we have from the Friedel sum rule for the spectral density that the $T = 0$ resistivity $\rho(0) \sim \sin^2(\pi n_0/2)$. This is satisfied for all cases shown in Fig. 11 with the same accuracy that the Friedel sum rule was satisfied for the spectral density (discussed earlier and summarized in Table 1).

In the Kondo regime at low temperature $T \ll T_{\rm K}$ the resistivity is given by the exact Fermi liquid result [30, 31, 32]

$$\rho(T) = \rho(0) \left\{ 1 - c \left(\frac{T}{T_{\rm K}} \right)^2 \right\}, \tag{44}$$

where $c = \frac{\pi^4}{16} = 6.088$ with corrections which increase with increasing asymmetry, as indicated in the previous section. The rescaled resistivity in the Kondo regime is shown in Fig. 13. Universal behaviour is found in the range $0 \le T \le 5T_{\rm K}$. The inset shows the expected T^2 Fermi liquid behaviour. In the Kondo regime the values of the T^2 coefficient extracted from a least squares fit in the region $0 \le T \le 0.1T_{\rm K}$ are within about 8% of the exact result $c = 6.088$ (see Table 1). The values of c increase systematically with increasing asymmetry and we believe this is in part due to the correction terms discussed previously. However the increase in c is small, less than 8% in going from the symmetric to the $\epsilon_0 = -2\Delta$ case, which indicates that the correction terms discussed earlier are also small in the Kondo regime.

At high temperatures $T \gg T_{\rm K}$, the resistivity is well described by the Hamann result [36] for the sum over parquet diagrams,

$$\rho(T) = \frac{\rho(0)}{2} \left(1 - \frac{\ln(T/T_{\rm KH})}{[(\ln(T/T_{\rm KH})^2 + \pi^2 S(S+1)]^{1/2}} \right). \tag{45}$$

Fig. 12 shows the resistivity for the symmetric case together with a fit of the Hamann result with $T_{\rm KH} = T_{\rm K}/1.2$. The fit is very good in the range $T_{\rm K} \leq T \leq 10T_{\rm K}$ but (45) fails to give the correct Fermi liquid behaviour at low temperature.

The effect of non–resonant scattering on the resistivity is shown in Fig. 14 for the symmetric case. The resistivity decreases slightly at low temperature for increasing absolute values of the non–resonant phase shift $|\eta_1|$. The overall behaviour, however, for small values of $|\eta_1|$ is the same as for resonant scattering only. The decrease with increasing $|\eta_1|$ is due to the induced change in the local charge δn away from $n_0 = 1$. Since the resistivity attains its maximum for $n_0 = 1$, any change away from this leads to a smaller resistivity. In the asymmetric case, the effect of non–resonant scattering is to decrease the resistivity for increasingly negative values of η_1 and to increase it for increasingly positive values of η_1. This effect is also due to the induced change in the local charge due to a repulsive ($\eta_1 > 0$) or attractive ($\eta_1 < 0$) local potential.

To summarize, the resistivity is described accurately over the whole range of temperatures from the logarithmically dominated region $T \gg T_{\rm K}$ through the crossover region $T \sim T_{\rm K}$ and into the low temperature Fermi liquid region $T \ll T_{\rm K}$.

Thermopower The thermopower is shown in Fig. 15–17 for the case of resonant scattering only. The effect of non–resonant scattering on the thermopower is discussed below. In Fig. 15 we show the low temperature Fermi liquid behaviour of the thermopower given by (26), $S(T)/\gamma T = (\pi/e)\cot(\pi n_0/2)$, which relates the linear coefficients of the thermopower and specific heat to the resonant level occupancy. By extracting γ from the second derivative $-\lim_{T\longrightarrow 0}\partial^2 F_{\rm imp}(T)/\partial T^2$ of the impurity Free energy and n_0 from the spectral density or partition function we have shown elsewhere [24] that this Fermi liquid relation is satisfied to a high degree of accuracy in all parameter regimes§.

From Fig. 16–17 it can be seen that the thermopower has different characteristic behaviour in the Kondo and mixed valency regimes. The thermopower for the symmetric case, $\epsilon_0 = -U/2$, is identically zero due to particle–hole symmetry (see later for a discussion of the effect of the non–resonant terms in this case). For the asymmetric case in the Kondo regime ($\epsilon_0/\Delta = -4, -3, -2$) it exhibits a low temperature maximum at $T \approx T_{\rm K}/3$ and then changes sign for $T > T_{\rm K}$ before reaching a broad minimum at high temperature $k_{\rm B}T \approx \Delta$ (Fig. 16). In the mixed valency regime ($\epsilon_0/\Delta = -1, 0$) there is again a maximum, at $k_{\rm B}T \approx \Delta/3$, but there is no sign change at higher temperature and there is only a shallow minimum at $k_{\rm B}T \approx \Delta$ (Fig. 17). The behaviour in the empty orbital regime ($\epsilon_0/\Delta = +1$) is similar to that in the mixed valency regime except that the shallow minimum at $k_{\rm B}T \approx \tilde{\epsilon_0} \approx \Delta$ becomes a shoulder (Fig. 17).

This complicated behaviour of the thermopower has a clear interpretation in terms of the temperature dependence of the spectral densities. We consider first the Kondo regime. The low temperature behaviour $T \ll T_{\rm K}$ of the thermopower obtained from

§ In the inset to Fig. 4 of [24] the curves $S(T)/T$ were labelled in the reverse order to the correct one shown here for different local level positions

the Sommerfeld expansion $S(T) \sim \gamma T$ shows that S is positive and large due to the strongly enhanced values of γ in the Kondo regime ($\gamma \sim 1/T_{\rm K}$). At temperatures T of order $T_{\rm K}$ for which the thermopower is determined by the Kondo resonance, we see from (5) that the sign of the thermopower depends on the slope of the spectral density at the Fermi level $\left(\frac{\partial \rho_0(\omega,T)}{\partial \omega}\right)_{\omega=\epsilon_{\rm F}}$. This slope decreases and eventually changes sign for $T > T_{\rm K}$ as a result of the strong temperature dependence of the Kondo resonance. This sign change at $T \approx T_{\rm K}$ is characteristic of the Kondo regime. As the temperature is increased to $k_{\rm B}T \approx \Delta$, charge fluctuations become increasingly more important and there is a transfer of spectral weight from the lower satellite peak at ϵ_0 to the upper one at $\epsilon_0 + U$ (Fig. 7). Holes are scattered increasingly more than electrons as the temperature is increased and therefore the thermopower increases for $k_{\rm B}T > \Delta$. Hence a broad minimum arises at $k_{\rm B}T \approx \Delta$.

The behaviour of the thermopower in the mixed valency and empty orbital regimes can be explained in a similar way in terms of the temperature dependence of the spectral density. In the mixed valency regime the interactions renormalize the bare local level ϵ_0 to lie at $\tilde{\epsilon_0}$ above the Fermi level (see Fig. 8). The thermopower can be analyzed in terms of the resonance at $\tilde{\epsilon_0}$ of width Δ in a similar way to the above analysis for the Kondo resonance. The low temperature maximum occurs at $k_{\rm B}T \approx \Delta/3$ but the low temperature enhancement $S(T) \sim \gamma T$ is only of order $\gamma \sim 1/\Delta$ (neglecting the phase factor $\cot(\pi n_0/2)$) . There is a maximum at $k_{\rm B}T \approx \Delta$, beyond which the thermopower decreases. In this case however, the resonance above the Fermi level does not disappear but is increasingly broadened with temperature (see Fig. 9). Hence the thermopower does not change sign. In the empty orbital regime, the behaviour of the thermopower can be similarly explained in terms of the temperature dependence of the spectral density.

We now consider the effect of non–resonant scattering of conduction electrons on the thermopower. The effects of non–resonant scattering are most dramatic for the symmetric case, where in the absence of such scattering the thermopower vanishes identically. The presence of non–resonant scattering leads to interference effects between the resonant $l = 0$ channel and non–resonant $l = 1$ channels making the thermopower finite even for the symmetric case (see Appendix A for details of how these interference terms arise). This is seen explicitly at low temperatures by applying the Sommerfeld expansion to (5) keeping the full transport time with inclusion of non–resonant terms,

$$S(T) = \frac{\pi\gamma\, T}{|e|}\left[\frac{\sin(2\eta_0(\epsilon_{\rm F}) - 2\eta_1)}{\sin^2(\eta_0(\epsilon_{\rm F}) - \eta_1) + \rho_n}\right] + O(T^3). \tag{46}$$

Here, $\eta_0(\omega)$ is the resonant phase shift,

$$\tan[\eta_0(\omega)] = -\frac{Im\; G_0(\omega)}{Re\; G_0(\omega)}, \tag{47}$$

and η_1 is the phase–shift of conduction electrons scattering in the $l = 1$ channel (ρ_n contains the effects of higher angular momentum scattering and was discussed earlier). For $\eta_0(\epsilon_{\rm F}) = \pi/2$ corresponding to the symmetric case the above expression gives a finite thermopower due to the non–resonant terms.

In Fig. 18 the thermopower for the symmetric case and several values of the non–resonant phase shift η_1 is shown. The thermopower can be positive or negative at low temperature depending on whether η_1 is negative or positive. This is clear since a positive η_1 corresponds to a repulsive potential which decreases the charge on the impurity making the thermopower the same as for less than half–filling, i.e. positive at low temperature and conversely for η_1 negative.

The effect of non–resonant scattering of conduction electrons on the thermopower in the asymmetric cases is shown in Fig. 19 and Fig. 20 for the Kondo and mixed valency cases respectively. In the mixed valency case we see that a small positive non–resonant phase shift can change the minimum at $k_{\rm B}T \approx \Delta$ (Fig. 20) into a shoulder making the thermopower resemble that of the empty orbital case. On the other hand a small negative non–resonant phase shift accentuates the minimum at $k_{\rm B}T \approx \Delta$ and makes the thermopower more similar to that of the Kondo case. It is possible that a sufficiently large negative phase shift η_1 could make the thermopower in the mixed valency case change sign, but in this case, which corresponds to strong non–resonant scattering, the frequency dependence of η_1 should be taken into account. In the Kondo regime similar trends are found on varying the non–resonant phase shift from negative to positive values. In the weak Kondo regime, $\epsilon_0/\Delta = -2$ (Fig. 19), for which $T_{\rm K} = 0.18\Delta$, a sufficiently large value for $\eta_1 > 0.042$ can change the sign of the high energy minimum at $k_{\rm B}T \approx \Delta$ making the thermopower resemble that of the mixed valency case. The effects of non–resonant scattering can be understood as for the symmetric case as arising from a change in the local screening charge on the impurity. A difference in the thermopower of Fig. 18 for the symmetric case and Fig. 19 for the asymmetric case is that the extremum at $k_{\rm B}T \approx \Delta$ in the symmetric case is very much suppressed. This is expected since this extremum is associated with the charge fluctuations which in the symmetric case are strongly suppressed and only included in the present case as a result of the non–resonant scattering terms. We see then that the thermopower is sensitive to small changes in the local environment of the magnetic ion which has been modelled here by including non–resonant scattering of conduction electrons. The sensitivity arises because of interference between the $l = 1$ channel and the resonant $l = 0$ channel, in contrast to the $l > 1$ channels which have negligible influence since they do not couple to the resonant channel.

Thermal Conductivity and Lorenz number The thermal conductivity is shown in Fig. 21. It shows the expected Fermi liquid behaviour $\kappa(T)/\alpha T \sim 1 + \beta(T/T_{\rm K})^2$ at low temperature ($T \ll T_{\rm K}$) with linear coefficient $\alpha \sim \tau(\epsilon_{\rm F}) \sim 1/\sin^2(\pi n_0/2)$ as shown in Fig. 22 and in accordance with the Friedel sum rule. The T^2 coefficient β, i.e. the T^3 coefficient of $\kappa(T)$, has also been extracted from the numerical results by using a least squares fit in the region $0 \leq T/T_{\rm K} \leq 0.01$. The T^2 behaviour is shown in Fig. 23 and the results extracted for β are listed in Table 1. It lies within 15–25 % of the exact result $\beta = 15.83$ calculated above using Fermi liquid theory. The agreement is surprisingly good since we are dealing with T^3 corrections to $\kappa(T)$ and the extraction of β also relies

on an accurate extraction of the linear coefficient α. The resistivity coefficient comes from a T^2 term and is consequently more accurate. A distinct low temperature anomaly is absent from $\kappa(T)$, and its behaviour is similar in both the Kondo and mixed valency regimes. Universality in $\kappa(T)/T$ extends up to at least $10T_{\rm K}$ in the Kondo regime. The Lorenz number ratio L/L_0 where $L = \kappa\rho/T$ and $L_0 = \pi^2 k_B/3e$ is shown in Fig. 24. Deviations from the Wiedemann–Franz law are found for $T \geq 0.1T_{\rm K}$. In the Kondo regime $L(T)$, like $\kappa(T)$, is universal up to approximately $10T_{\rm K}$. In the Kondo regime it also exhibits a maximum at $T \approx T_{\rm K}$ whereas in the mixed valency there is only a shoulder at $k_{\rm B}T \approx \Delta$, and similarly in the empty orbital regime. The inclusion of weak non–resonant scattering has little effect on $\kappa(T)$.

Hall coefficient Fig. 25 shows the temperature dependence of the Hall coefficient. This quantity exhibits a low temperature peak at $T \approx T_{\rm K}$ in the Kondo regime but not in the mixed valency or empty orbital regimes. Universality for this quantity persists only up to $T \approx T_{\rm K}$. Here we have only considered the ordinary Hall effect and have shown that this exhibits an anomaly at $T \approx T_{\rm K}$. A more important contribution to the Hall effect arises from skew scattering of conduction electrons. Up spin electrons are scattered differently in a magnetic field than down spin electrons as a result of the splitting of the Kondo resonance by the magnetic field. This contribution should be much more important than that coming from the Lorenz term considered here, but its treatment is outside the scope of the present work.

Discussion and Conclusions

In this paper we have given a detailed description of the generalization of the numerical renormalization group to the calculation of finite temperature Green's functions of the Anderson model. The method was applied to obtain the single–particle spectral densities and transport properties of the Anderson model in the strong correlation limit $U/\pi\Delta \gg 1$ for a range of temperatures and parameter regimes, as well as the occupation number and specific heat. We distinguish three parameter regimes in the limit of strong correlation. The Kondo regime, $\epsilon_0 \ll -\Delta,\ n_0 \approx 1$, characterized by a low energy scale $k_B T_0 = k_B T_{\rm K}$, the valence fluctuation regime, $-\Delta \leq \epsilon_0 \leq 0,\ 0.3 \leq n_0 \leq 0.8$, characterized by a low energy scale $k_B T_0 = \Delta$, and the empty orbital regime, $\epsilon_0 \geq \Delta,\ n_0 < 0.3$, characterized by an energy scale $k_B T_0 \sim \tilde{\epsilon_0} \sim \epsilon_0$. We also distinguish three temperature ranges, $T \ll T_0$ corresponding to the Fermi liquid regime, $T \gg T_0$ corresponding to the high temperature perturbative regime and $T \approx T_0$ corresponding to the cross–over region. A consistent picture of the thermodynamics, spectral densities and transport coefficients emerges from the numerical renormalization group calculations in these different regimes.

The calculations of the single particle excitation spectrum show that at low temperatures the spectral function in the Kondo regime is characterized by a Kondo resonance of negligible spectral weight, centered around $\epsilon_{\rm F}$, and two atomic like

resonances at ϵ_0 and $\epsilon_0 + U$, which carry most of the spectral weight. The one below the Fermi level at ϵ_0 contains most of the screening charge while the one above at $\epsilon_0 + U$ is empty. This picture is well known and emerged very clearly in the finite order perturbation calculations of Yamada [31]. Using the numerical renormalization technique we have been able to calculate it more accurately and obtain the correct exponential dependence of the width $T_{\rm K}$ on ϵ_0 and U and also describe the high temperature regime where there are corrections that depend logarithmically on T.

The spectral function for valence fluctuators is characterized by two peaks only: a partially filled one at the renormalized position $\tilde{\epsilon_0} > \epsilon_{\rm F}$ and an empty one at $\tilde{\epsilon_0} + U$. In the empty orbital regime the low temperature spectral function in the strong coupling limit is just an empty virtual bound state. The characteristic low energy scale for the spectral function is set by T_0. These features of the spectral density are fully consistent with the Fermi liquid groundstate as revealed by the thermodyamics [2]. The Friedel sum rule which is a good test on the accuracy of the method at both high and low energies was found to be satisfied to within 3% accuracy in all parameter regimes. Increase of temperature leads to a renormalization of the excitation spectrum and for $T > T_0$ the spectral function changes in a qualitative way [7]. At high temperatures the spectral function is characterized by two atomic like peaks separated in energy by U, consistent with the thermodynamic properties which exhibit local moment behaviour. In the mixed valency and empty orbital regimes the higher peak is strongly suppressed.

The transport coefficients for the Anderson model can be related to the transport relaxation time by using linear response theory. This can be further related to the single particle spectral function which allows us to discuss the transport coefficients in terms of elementary excitations in the resonant channel. The characteristic low energy scale of the spectral function, T_0, defines the temperature scale for transport properties.

In the Kondo regime at low temperature, $T \ll T_0 = T_{\rm K}$, we showed that the transport coefficients agreed with the predictions of Fermi liquid theory. For $T \ll T_{\rm K}$, the localized spins are screened and the transport currents relax via excitations in the local Fermi liquid state formed by the Kondo screening mechanism. The transport coefficients were characterized by power law dependencies on $T/T_{\rm K}$ (34–37) with universal coefficients for appropriately scaled quantities. The numerical results for the T^2 term of the resistivity and the T^3 term of the thermal conductivity in the symmetric case agreed remarkably well with the analytic values deduced from Fermi liquid theory. With increasing asymmetry the numerical results indicate that these coefficients change but only slightly for $n_0 > 0.8$. The thermopower shows universal behaviour for $T \leq T_{\rm K}$ when rescaled by its zero temperature slope [26]. Universality was found to extend up to at least $10T_{\rm K}$ for the resistivity and thermal conductivity but only up to $T_{\rm K}$ for the Hall coefficient. The transport properties in this regime are understood in terms of excitations in the strongly renormalized Fermi liquid ground state. On increasing temperature through the cross–over region $T \approx T_{\rm K}$ logarithmic terms become important for the resistivity and these are clearly seen for $T > T_{\rm K}$. The thermopower changes sign, a result of the disappearance for $T > T_{\rm K}$ of the Kondo resonance in the single–

particle spectral density. There is also a minimum in the Hall coefficient at $T \approx T_{\rm K}$. In the high temperature perturbative regime, $T \gg T_{\rm K}$, the spectral density consists of two peaks, the occupancy n_0 approaches 1 and the transport properties are those of electrons coupled weakly to local spins. The thermopower develops a broad minimum at $k_{\rm B}T \approx \Delta$ due to a shift of spectral weight from the peak below the Fermi level to that above as charge fluctuations become important.

In the mixed valency and empty orbital regimes the transport coefficients at low temperature $T \ll T_0$ again reflect the relaxation of the transport currents via the excitations in the renormalized local Fermi liquid ground state. However, since $\Delta \gg k_{\rm B}T_{\rm K}$, these renormalizations of order $1/T_0$ are smaller than for the Kondo case. The low temperature transport coefficients again have power law dependencies on T/T_0, but the coefficients are non–universal and depend strongly on the occupation of the localized level n_0.

Finally, we investigated the effects of non–resonant scattering of conduction electrons on the temperature dependence of the transport properties. A general expression for the transport time in the presence of such scattering was derived which shows that the resulting interference effects between the resonant and non–resonant channels are not negligible. Hence, to relate the transport coefficients of the Anderson model to the experimental data on dilute alloys one should take into account the non–resonant scattering. For example, the overall shape of the thermopower curves calculated for the Anderson model with two scattering channels resembles quite strikingly the experimental data. The interference effects between resonant and non–resonant scattering channels led to a strong dependence of the sign of the thermopower on the non–resonant phase shift. This type of effect could be important for systems with n_0 close to 1 or for systems with a Kondo resonance approximately symmetric about the Fermi level. Doping such systems with non–magnetic impurities could lead to the above type of interference effects making the sign of the thermopower sensitive to the local environment. Such effects have been observed [41] In the symmetric Kondo regime the inclusion of non–resonant scattering was important to obtain the non–vanishing enhanced thermopowers for half–filled systems (the $n_0 = 1$).

To summarize, we have shown that the numerical renormalization group method allows a unified description of the transport, thermodynamic and spectral properties of the Anderson model in the strong correlation limit. The different features below and above the characteristic scale T_0 reflect differences in the structure of the excitation spectrum at high and low temperatures. The NRG method presented here could be used to provide further insights into the behaviour of the Anderson model. For instance, the results for the spectral density could be used to deduce the spin and charge densities induced in the conduction electrons at arbitrary distances from the impurity [42]. The interference effects for the transport properties could also be studied for two Kondo (spin 1/2) impurities or for the case of the Kondo effect in the $l = 0$ channel and a virtual bound state in the $l = 1$ channel. This would be relevant to rare earth systems in which there is an excited crystal electric field level close to the Kondo ground state.

There are many other similarly interesting physical situations which occur in particular materials. They could be modelled and a broad range of physical properties calculated via this one technique to compare with experiment.

0.1. Acknowledgments

We acknowledge the support of an SERC grant, and the Computational Science Initiative for Computer equipment. One of us (TAC) would like to thank Prof. E. Müller–Hartmann for making possible a visit to the Institute for Theoretical Physics at Cologne University where part of this work was carried out. Financial support from the *Institute of Physics of the University of Zagreb*, (VZ,TAC), the British Council (TAC) and the *Graduiertenkolleg Festkörperspektroskopie, University of Dortmund*, (TAC), is also acknowledged.

Appendix A. Derivation of the transport time in the presence of non–resonant scattering

The transport time for scattering from a dilute concentration, $n_i \ll 1$, of magnetic impurities described by the Hamiltonian (1) can be obtained by examining the Kubo expression for the conductivity $\sigma(T)$,

$$\sigma(T) = -\lim_{\omega\to 0}\frac{1}{\omega}\,\mathrm{Im}\,\Pi_{\rm ret}(\omega), \tag{A.1}$$

where the current–current correlation function $\Pi(i\omega) = -\frac{1}{3V}\int_0^\beta e^{i\omega\tau}\langle T_\tau \mathbf{j}(\tau)\mathbf{j}(0)\rangle$ and the current operator is that for free–electrons $\mathbf{j} = -\frac{e}{m}\sum_{\mathbf{k}\sigma}\mathbf{k}\; c^\dagger_{\mathbf{k}\sigma}c_{\mathbf{k}\sigma}$. The diagrammatic representation of $\Pi(i\omega_n)$ is shown in Fig. 26. In the absence of non–resonant scattering the vertex corrections vanish identically [13] in the dilute limit leaving just the (dressed) bubble diagram Π_0. In terms of the dressed conduction electron Green's function $G(\mathbf{k},\omega)$ this is

$$\Pi_0(i\omega) = \frac{2e^2}{3m^2V}\sum_{\mathbf{k}}\mathbf{k}^2\frac{1}{\beta}\sum_{i\omega_n}G(\mathbf{k},i\omega_n+i\omega)G(\mathbf{k},i\omega_n). \tag{A.2}$$

Here we evaluate the conductivity including the vertex corrections since these give rise to interference terms between the $l=0$ and $l=1$ channels. The conductivity is given by [28]

$$\sigma(T) = \frac{1}{2\pi}\int_{-\infty}^{+\infty}\left(\frac{-\partial f}{\partial\epsilon}\right)\left[P(\epsilon-i\delta,\epsilon+i\delta) - Re[P(\epsilon+i\delta,\epsilon+i\delta)]\right]d\epsilon, \tag{A.3}$$

where the singular part behaving like $1/n_i$ comes from the first term with $P(\epsilon-i\delta,\epsilon+i\delta)$ [28]. The latter is given in terms of the conduction electron Green's function $G(\mathbf{k},\epsilon)$ and vector vertex function $\mathbf{\Gamma}$ by

$$P(\epsilon-i\delta,\epsilon+i\delta) = \frac{2e^2}{3m^2}\frac{1}{V}\sum_k G(\mathbf{k},\epsilon+i\delta)G(\mathbf{k},\epsilon-i\delta)\mathbf{k}.\mathbf{\Gamma}(\mathbf{k},\epsilon-i\delta,\epsilon+i\delta). \tag{A.4}$$

The vertex function $\mathbf{\Gamma}$ satisfies the following equation

$$\mathbf{\Gamma}(\mathbf{k},\epsilon-i\delta,\epsilon+i\delta)=\mathbf{k}+\int\frac{d^3\mathbf{k}'}{(2\pi)^3}\mathbf{\Gamma}(\mathbf{k}',\epsilon-i\delta,\epsilon+i\delta)W_{\mathbf{k}\mathbf{k}'}(\epsilon-i\delta,\epsilon+i\delta)$$
$$\times G(\mathbf{k}',\epsilon-i\delta)G(\mathbf{k}',\epsilon+i\delta) \tag{A.5}$$

where W is the irreducible vertex.

To solve this equation we introduce a scalar vertex function γ_1 defined by $\mathbf{\Gamma}(\mathbf{k},\epsilon-i\delta,\epsilon+i\delta)=\mathbf{k}\ \gamma_1(\mathbf{k},\epsilon)$ and note that the Green's function product in (A.5) is just $A(\mathbf{k},\epsilon)/|\Sigma^I(\mathbf{k},\epsilon)|$ where $A(\mathbf{k},\epsilon)$ is the spectral density and $\Sigma^I(\mathbf{k},\epsilon)$ the imaginary part of the self–energy of the conduction electrons. In the dilute limit, $n_i\to 0$, we also have that [28] $W_{\mathbf{k}\mathbf{k}'}(\epsilon-i\delta,\epsilon+i\delta)\to n_i T_{\mathbf{k}\mathbf{k}'}(\epsilon-i\delta)T_{\mathbf{k}'\mathbf{k}}(\epsilon+i\delta)$, where T is the energy dependent T–matrix, $|\Sigma^I(\mathbf{k}',\epsilon_{\mathbf{k}'})|\to n_i|ImT_{\mathbf{k}'\mathbf{k}'}|$ and $A(\mathbf{k}',\epsilon)\to 2\pi\delta(\epsilon-\epsilon_{\mathbf{k}'})$. The resulting equation for the scalar vertex function after some algebra becomes

$$\gamma_1(\mathbf{k},\epsilon)=1+$$
$$\frac{m}{4\pi}\int d\epsilon_{\mathbf{k}'}d\theta'\sqrt{2m\epsilon_{\mathbf{k}'}}\frac{\sin\theta'\cos\theta'\delta(\epsilon-\epsilon_{\mathbf{k}'})T_{\mathbf{k}\mathbf{k}'}(\epsilon-i\delta)T_{\mathbf{k}'\mathbf{k}}(\epsilon+i\delta)\gamma_1(\mathbf{k}',\epsilon)}{|Im\,T_{\mathbf{k}'\mathbf{k}'}(\epsilon+i\delta)|} \tag{A.6}$$

where θ' defined by $\cos(\theta')=\mathbf{k}.\mathbf{k}'/\mathbf{k}^2$ is the angle between incoming and scattered k states and a free electron density of states has been used to rewrite the integrals. The T–matrix in the denominator of (A.6) is for forward scattering only so it is independent of θ' and can therefore be taken outside the integral and evaluated at $k'=k$ (note the δ function in (A.6)). The scalar vertex function $\gamma_1(\mathbf{k}',\epsilon)$ is also independent of angle and can also be taken outside the integral (evaluated at $k'=k$). Hence the closed expression,

$$\gamma_1(k,\epsilon)=1+\frac{mk}{4\pi}\frac{I_k}{|Im\,T_{kk}(\epsilon_k+i\delta)|}\gamma_1(k,\epsilon), \tag{A.7}$$

is obtained with solution,

$$\gamma_1(k,\epsilon_k)=\frac{|Im\,T_{kk}(\epsilon_k+i\delta)|}{|Im\,T_{kk}(\epsilon_k+i\delta)|-\frac{mk}{4\pi}I_k}, \tag{A.8}$$

In the above expressions I_k given by

$$I_k=\int_0^\pi d\theta'\sin\theta'\cos\theta' T_{\mathbf{k}\mathbf{k}'}(\epsilon_{\mathbf{k}}-i\delta)T_{\mathbf{k}'\mathbf{k}}(\epsilon_{\mathbf{k}}+i\delta) \tag{A.9}$$

contains the interference effects.

Substituting the scalar vertex function γ_1 from (A.8) into the expression for $P(\epsilon-i\delta,\ \epsilon+i\delta)$ (using the previosuly quoted expression for the Green's function product) gives

$$P(\epsilon-i\delta,\epsilon+i\delta)=\frac{2e^2}{3m^2}\frac{1}{V}\sum_{\mathbf{k}}k^2A(\mathbf{k},\epsilon)\gamma_1(k,\epsilon)/\Sigma^I(\mathbf{k},\epsilon) \tag{A.10}$$

and the latter into the conductivity formula (A.1) gives for the transport time τ the expression

$$\tau(\epsilon_k,T)^{-1}=2n_i(|Im\,T_{kk}(\epsilon_k+i\delta)|-\frac{mk}{4\pi}I_k). \tag{A.11}$$

The first part of this expression is just the usual result for s–wave scattering only and the second part is the contribution coming from interference effects between the resonant $l = 0$ channel and the non–resonant channels. To evaluate (A.9) and (A.11) we need the T–matrix. This can be obtained for the Hamiltonian (1) by aplying the equation of motion method to the conduction electron Green's function $G_{\mathbf{k}\mathbf{k}'\sigma} = \langle\langle c_{\mathbf{k}\sigma}; c^{\dagger}_{k'\sigma}\rangle\rangle$. This gives

$$G_{\mathbf{k}\mathbf{k}'\sigma}(\omega+i\delta) = G^0_{\mathbf{k}\mathbf{k}'\sigma}(\omega+i\delta)+G^0_{\mathbf{k}\mathbf{k}'\sigma}(\omega+i\delta)T_{\mathbf{k}\mathbf{k}'}(\omega+i\delta)G^0_{\mathbf{k}\mathbf{k}'\sigma}(\omega+i\delta), \quad \text{(A.12)}$$

where

$$T_{\mathbf{k}\mathbf{k}'}(\omega + i\delta) = V_{0\mathbf{k}}G_0(\omega + i\delta)V_{0\mathbf{k}'} + \sum_{l=1,m} V_{lm\mathbf{k}}G_l(\omega + i\delta)V_{lm\mathbf{k}'}, \quad \text{(A.13)}$$

$G^0_{\mathbf{k}\mathbf{k}'\sigma}$ is the unperturbed conduction electron Green's function and $G_l, l = 0, 1, \ldots$ are the local Green's functions for the $l = 0, 1, \ldots$ channels respectively. The hybridization matrix elements $V_{lm\mathbf{k}}$ have the angular dependence $V_{lm\mathbf{k}} = \langle k|V|l, m\rangle \sim V_{lk}Y_{lm}(\Omega_{\mathbf{k}})$ so the T matrix has the form:

$$T_{\mathbf{k}\mathbf{k}'}(\omega + i\delta) = \sum_{l=0}(2l + 1)P_l(\cos(\theta'))V_{lk}G_l(\omega + i\delta)V_{lk'} \quad \text{(A.14)}$$

$$= V_{0k}G_0(\omega + i\delta)V_{0k'} + 3\cos(\theta')V_{1k}G_1(\omega + i\delta)V_{1k'} + \ldots \quad \text{(A.15)}$$

$$\quad \text{(A.16)}$$

where $\sum_m Y_{lm}(\Omega_k)Y_{lm}(\Omega_{k'}) \sim (2l+1)P_l(\cos(\theta'))$ has been used and $\theta' = \mathbf{k}.\mathbf{k}'/\mathbf{k}^2$. The T matrix has an explicit dependence on the angle θ' which gives rise to interference effects between the resonant and non–resonant channels when substituted into the expression for the transport time (A.11). These interference effects arise in the expression for I_k as cross–terms involving $G^*_0G_1 + G_0G^*_1$. On carrying out the θ' integrations in (A.9) and expressing the non–resonant Green's function $G_1(\omega)$ in terms of a corresponding phase shift $\eta_1(\omega)$ we arrive at the formula for the transport time of the multi–channel Anderson impurity model:

$$\frac{1}{\tau(\omega, T)} = \frac{1}{\tau^0(\omega, T)}\left[\cos 2\eta_1 - \frac{Re\ G_0(\omega, T)}{\text{Im}\ \ G_0(\omega, T)}\sin 2\eta_1\right] + \rho_n. \quad \text{(A.17)}$$

The resonant part of the transport time, $\tau_0(\omega, T)$ is given by the usual T–matrix expression in the absence of the interference effects,

$$\frac{1}{\tau_0(\omega, T)} = \Delta\rho_0(\omega, T) = -\Delta\ \text{Im}\ G_0(\omega, T)/\pi, \quad \text{(A.18)}$$

where, Δ is the unrenormalized width of the $l = 0$ resonance and $G_0(\omega, T)$ is the $l = 0$ Green's function, which describes the many–body effects. The analysis here was for the electrical conductivity. The same transport time (A.17) is found by repeating this analysis for the other current–current correlation functions (In the above expressions for the inverse transport times, a constant factor $2n_i/N(0)$, where $N(0)$ is the unperturbed conduction electron density of states at the Fermi level, has been omitted).

Appendix B. The Numerical Renormalization Group Method

The following continuum version for the resonant part of (1) is useful for introducing the logarithmic discretization approximation [2],

$$H = \epsilon_0 c^\dagger_{0\sigma} c_{0\sigma} + U n_{0\uparrow} n_{0\downarrow} + V_0 \int_{-1}^{+1} dk (c^\dagger_{k\sigma} c_{0\sigma} + c^\dagger_{0\sigma} c_{k\sigma}) + \int_{-1}^{+1} k c^\dagger_{k\sigma} c_{k\sigma} dk. \quad \text{(B.1)}$$

In obtaining this from the resonant part of (1), a partial wave expansion for the conduction states around the impurity has been used has been used and the Hamiltonian has been written in the energy representation. The approximation has been made that $\Delta(\omega) = \pi \sum_k |V_{0k}|^2 \delta(\omega - \epsilon_k) = \Delta$ is independent of frequency so that only s–wave partial wave states couple to the impurity (with strength $V_0 = \sqrt{\Delta/\pi N(\epsilon_{\rm F})}$). All energies are measured relative to the half bandwidth $D = 1$ and we use the convention that repeated spin indices are summed over. (full details of the above may be found in [2]). The continuum conduction band $[-1, 1]$ is now discretized as shown in Fig. 27 and a new set of basis states for the conduction electrons is introduced in each interval $\pm[\Lambda^{-(n+1)}, \Lambda^{-n}]$ using the following wavefunctions

$$\psi^{\pm}_{np}(k) = \begin{cases} \frac{\Lambda^{n/2}}{D(1-1/\Lambda)^{1/2}} e^{\pm i\omega_n pk} & \text{for } \Lambda^{-n-1} < \pm k < \Lambda^{-n} \\ 0 & \text{otherwise} \end{cases} \quad \text{(B.2)}$$

Here p is a Fourier harmonic index and $\omega_n = 2\pi\Lambda^n/(1 - \Lambda^{-1})$. The operators $c_{k\sigma}$ can then be expanded in terms of new operators $a_{np\sigma}, b_{np\sigma}$ labelled by the interval n and the harmonic index p

$$c_{\mathbf{k}\sigma} = \sum_{np} [a_{np\sigma} \psi^+_{np} + b_{np\sigma} \psi^-_{np}]. \quad \text{(B.3)}$$

In terms of these operators, the Hamiltonian (B.1) becomes [2],

$$\begin{aligned} H &= \epsilon_0 c^\dagger_{0\sigma} c_{0\sigma} + U n_{0\uparrow} n_{0\downarrow} \\ &+ V_0 (1 + \Lambda^{-1})^{1/2} \sum_{n=0}^{\infty} \Lambda^{-n/2} ((a^\dagger_{n0\sigma} + b^\dagger_{n0\sigma}) c_{0\sigma} + c^\dagger_{0\sigma} (a_{n0\sigma} + b_{n0\sigma})) \\ &+ \frac{1}{2}(1 + \Lambda^{-1}) \sum_{np} \Lambda^{-n} (a^\dagger_{np\sigma} a_{np\sigma} - b^\dagger_{np\sigma} b_{np\sigma}) \\ &+ \frac{(1 - \Lambda^{-1})}{2\pi i} \sum_n \sum_{p \neq p'} \Lambda^{-n} (a^\dagger_{np\sigma} a_{np'\sigma} - b^\dagger_{np\sigma} b_{np'\sigma}) e^{\frac{2\pi i (p-p')}{(1-\Lambda^{-1})}}. \end{aligned} \quad \text{(B.4)}$$

The coupling of the local state $c_{0\sigma}$ to just the $p = 0$ harmonic is a consequence of the assumption that the hybridization matrix elements are independent of energy. Hence the conduction electron orbitals a_{np}, b_{np} for $p \neq 0$ only couple to the impurity state $c_{0\sigma}$ indirectly via their coupling to the a_{n0}, b_{n0} in the last term of (B.4). This coupling is weak, being proportional to $(1 - \Lambda^{-1})$, and vanishes in the continuum limit $\Lambda \longrightarrow 1$, so these states may be expected to contribute little to the impurity properties compared to the $p = 0$ states. This is indeed the case as can be seen in Fig. 28, where the probability density in real space of the wave–packet states $\psi_{np}(k)$ is shown. It can be seen that the

$p\rangle 0$ orbitals are localized at increasing distances from the impurity, whereas the $p = 0$ orbitals overlap strongly with the impurity. This together with their weak coupling to the impurity ensures that they can be neglected in calculating local impurity properties. This *logarithmic discretization approximation* has been shown to give rapidly convergent results (as $\Lambda \longrightarrow 1$) for thermodynamic averages. The deviations away from the continuum limit, $\Lambda = 1$, being proportional to $e^{-\frac{\pi^2}{\ln(\Lambda)}}$ [1, 2]. The approximation amounts to approximating the continuum conduction band Hamiltonian $H_{\rm c}$, by a discrete one:

$$H_{\rm c} \approx \frac{1}{2}(1+\Lambda^{-1})\sum_n \Lambda^{-n}(a^\dagger_{n0\sigma}a_{n0\sigma} - b^\dagger_{n0\sigma}b_{n0\sigma}). \tag{B.5}$$

Consequently a discrete approximation to the Anderson model is obtained

$$\begin{aligned} H &= \epsilon_0 c^\dagger_{0\sigma}c_{0\sigma} + U n_{0\uparrow}n_{0\downarrow} \\ &+ V_0(1+\Lambda^{-1})^{1/2}\sum_{n=0}^{\infty}\Lambda^{-n/2}((a^\dagger_{n\sigma}+b^\dagger_{n\sigma})c_{0\sigma} + c^\dagger_{0\sigma}(a_{n\sigma}+b_{n\sigma})) \\ &+ \frac{1}{2}(1+\Lambda^{-1})\sum_n \Lambda^{-n}(a^\dagger_{n\sigma}a_{n\sigma} - b^\dagger_{n\sigma}b_{n\sigma}), \end{aligned} \tag{B.6}$$

where the p index has now been dropped since only $p = 0$ states are included. This discrete Hamiltonian is more convenient for a numerical treatment.

The next step is to convert the discrete Hamiltonian (B.6) into a linear chain form suitable for an iterative diagonalization starting from a small chain and diagonalizing sucessively longer chains by adding a site or energy shell at each stage. If we define a new local conduction electron orbital by $|0\sigma\rangle = f^\dagger_{0\sigma}|{\rm vac}\rangle$ where

$$f^\dagger_{0\sigma} = [\frac{1}{2}(1+\Lambda^{-1})]^{1/2}\sum_{n=0}^{\infty}\Lambda^{-n/2}((a^\dagger_{n\sigma}+b^\dagger_{n\sigma}), \tag{B.7}$$

then the Lanczos algorithm can be used with starting vector $|0\sigma\rangle$ to tri–diagonalize $H_{\rm c}$

$$H_{\rm c} = \sum_{n=0}^{\infty}\epsilon_n f^\dagger_{n\sigma}f_{n\sigma} + \sum_{n=0}^{\infty}\lambda_n(f^\dagger_{n+1\sigma}f_{n\sigma} + f^\dagger_{n\sigma}f_{n+1\sigma}), \tag{B.8}$$

where $\epsilon_n, \lambda_n, n = 0, 1, \ldots$ are the site and hopping energies respectively. For the half–filled Fermi sea $|{\rm vac}\rangle$ the ϵ_n are all zero and Wilson has obtained the expression $\lambda_n = \frac{1}{2}(1+\Lambda^{-1})\Lambda^{-n/2}\xi_n$, where $\xi_n = \xi_n(\Lambda) \to 1$ for $n \gg 1$. This converts (B.6) into a semi–infinite chain with the impurity at the origin coupled to the local conduction state $|0\sigma\rangle$ via the hybridization V_0 (re–scaled to keep $|0\sigma\rangle$ normalized)

$$\begin{aligned} H &= \epsilon_0 c^\dagger_{0\sigma}c_{0\sigma} + U n_{0\uparrow}n_{0\downarrow} + V_0(f^\dagger_{0\sigma}c_{0\sigma} + H.c.) \\ &+ \frac{1}{2}(1+\Lambda^{-1})\sum_{n=0}^{\infty}\lambda_n(f^\dagger_{n+1\sigma}f_{n\sigma} + f^\dagger_{n\sigma}f_{n+1\sigma}) \\ &= \lim_{N\to\infty}\frac{1}{2}(1+\Lambda^{-1})\Lambda^{-(N-1)/2}H_N \end{aligned} \tag{B.9}$$

$$H_N = \Lambda^{(N-1)/2}[H_0 + H_{\rm hyb} + \sum_{n=0}^{N-1}\Lambda^{-n/2}\xi_n(f^\dagger_{n+1\sigma}f_{n\sigma} + f^\dagger_{n\sigma}f_{n+1\sigma})]. \tag{B.10}$$

In (B.10) we have defined a sequence of rescaled Hamiltonians H_N whose smallest term is always of order 1 (the bare parameters ϵ_0, U, V_0 are also rescaled by the factor $\frac{1}{2}(1+\Lambda^{-1})$). The procedure is now to diagonalize this sequence of Hamiltonians iteratively and extract the spectrum and eigenstates on successively lower energy scales $\omega_N \sim \Lambda^{-(N-1)/2}$. The procedure starts by diagonalizing the impurity part, $H_0 = \epsilon_0 c^\dagger_{0\sigma} c_{0\sigma} + U n_{0\uparrow} n_{0\downarrow}$ of (B.9) and then adding the coupling to the local conduction electron orbital $V_0(f^\dagger_{0\sigma} c_{0\sigma} + H.c.)$. Successive energy shells $\lambda_n(f^\dagger_{n+1\sigma} f_{n\sigma} + f^\dagger_{n\sigma} f_{n+1\sigma}), n = 0, 1, \ldots$ are then added and the resulting Hamiltonian diagonalized to give the many–body eigenvalues E^N_p and eigenvectors $|p\rangle_N$ of the corresponding shell or cluster. The total number of electrons, N_e, total spin, S, and z–component of total spin, S_z, are conserved quantities and can be used to label the eigenstates together with an index $r = 1, R^N_{N_eS}$ where $R^N_{N_eS}$ is the dimension of the subspace (N_eS). If H_N has been diagonalized, $H_N = \sum_{N_eSS_zr} E^N_{N_eS} X^N_{N_eSS_zr,N_eSS_zr}$, then from (B.10) the matrix for H_{N+1} can be obtained from

$$H_{N+1} = \Lambda^{1/2} H_N + \xi_N (f^\dagger_{N+1\sigma} f_{N\sigma} + f^\dagger_{N\sigma} f_{N+1\sigma}). \tag{B.11}$$

The basis used for H_{N+1} is the product basis $|p, i\rangle$ of eigenstates, $|p\rangle = |N_eSS_zr\rangle$, of H_N, and states $|i\rangle$ from site $N+1$ (i.e. $|i >= |0\rangle, |\uparrow\rangle, |\downarrow\rangle, |\uparrow\downarrow\rangle$). In this basis the matrix elements of H_{N+1} are

$$\begin{aligned}
&\langle p, i|H_{N+1}|q, j\rangle = \Lambda^{1/2}\delta_{p,q}\delta_{i,j}E^N_p \\
&+ \xi_N(\langle p, i|f^\dagger_{N+1\sigma} f_{N\sigma}|q, j\rangle + \langle p, i|f^\dagger_{N\sigma} f_{N+1\sigma}|q, j\rangle) \\
&= \Lambda^{1/2}\delta_{p,q}\delta_{i,j}E^N_p + \xi_N(-1)^{N_{e,q}} \\
&\times (\langle i|f^\dagger_{N+1\sigma}|j\rangle\langle p|f_{N\sigma}|q\rangle + \langle p|f^\dagger_{N\sigma}|q\rangle\langle i|f_{N+1\sigma}|j\rangle),
\end{aligned} \tag{B.12}$$

where $f_{N+1\sigma}$ have been commuted past the eigenstates $|p\rangle, |q\rangle$ with a sign change $(-1)^{N_{e,q}}$ depending on the number of electrons, $N_{e,q} = N_{e,p}$, in these states. Since H_N is already diagonalized the matrix elements $\langle p|f_{N\sigma}|q\rangle$ can be calculated as follows. The unitary transformation between the eigenstates of H_N and the product basis is known and is given by

$$|p\rangle_N = \sum_{r,i} U_N(p, ri)|r\rangle_{N-1}|i\rangle, \tag{B.13}$$

where $U_N(p, ri)$ is the matrix of eigenvectors of H_N, $|r\rangle_{N-1}$ denotes an eigenvector of the previous cluster $(N-1)$ and $|i\rangle$ is one of the four states given above, but for site N (not $N+1$). Hence the required matrix elements are given by

$$\begin{aligned}
\langle p|f_{N\sigma}|qrangle_N &= \sum_{r,i}\sum_{r',i'} U^*_N(p, ri)U_N(p, r'i')\langle i|\langle r|f_{N\sigma}|r'\rangle|i'\rangle \\
&= \sum_{r,i}\sum_{r',i'} U^*_N(p, ri)U_N(q, r'i')\delta_{r,r'}(-1)^{N_{e,r}}\langle i|f_{N\sigma}|i'\rangle,
\end{aligned} \tag{B.14}$$

which involves only known expressions. The matrix elements $\langle i|f_{N+1\sigma}|j\rangle$ in (B.12) are also known so the matrix of H_{N+1} can be set up in terms of the eigenvalues and matrix elements in (B.14). H_{N+1} can then be diagonalized and the procedure repeated to obtain

the spectrum on successively lower energy scales, $\omega_{N+2}, \omega_{N+3}, \ldots$, where $\omega_N \approx D\Lambda^{-\frac{N-1}{2}}$ is the smallest scale in H_N. In practice since the number the number of many–body states in H_N grows like 4^N it is not possible to retain all states after about $N = 7$ (even after symmetry has been used to reduce the size of the matrices). For $N > 7$ only the lowest 1000 or so states of H_N are retained. The truncation of the spectrum in H_N restricts the reliable range of excitations ω to $\omega_N \leq \omega \leq K\omega_N$ where K is a constant dependent on Λ ($K \approx 10$ for $\Lambda = 3$). The lower excitations are calculated more reliably in successive iterations, whilst information on the higher excitations is contained in previous iterations. The eigenvalues are used to calculate the partition function $Z_N(\beta_N = 1/k_B T_N)$ and free energy $F(T_N) = -k_B \ln(Z_N(T_N))$ for the total system at a decreasing sequence of temperatures $T_N = \omega_N/k_B \sim D\Lambda^{-(N-1)/2}, N = 0, 1, \ldots$. The thermodynamic properties are then extracted by first subtracting out the conduction electron contribution to the free energy, $F_{\rm c}(T_N)$ [1, 2]. The specific heat is then given by the second derivative of the impurity free energy, $F_{\rm imp}(T) = F(T) - F_{\rm c}(T)$,

$$C(T) = -T\frac{\partial^2 F_{\rm imp}}{\partial T^2} \tag{B.15}$$

References

[1] Wilson K G *Rev. Mod. Phys.* 1975 **47** 773
[2] Krishnamurthy H R, Wilkins J W and Wilson K G 1980 *Phys. Rev.* B **21** 1044
[3] Hewson A C 1993 *The Kondo Problem to Heavy Fermions*, Cambridge Studies in Magnetism (Cambridge: Cambridge University Press)
[4] Schrieffer J R and Wolff P A 1966 *Phys. Rev.* **149** 491
[5] Andrei N, Furuya K and Lowenstein J H 1983 *Rev. Mod. Phys.* **55** 331
[6] Tsvelick A M and Wiegmann P B 1983 *Adv. Phys.* **32** 453
[7] Horvatić B, Šokčević D and Zlatić V 1987 *Phys. Rev.* B **36** 675
[8] Yamada K 1976 *Prog. Theor. Phys.* **55** 1345
[9] Friedel J 1952 *Phil. Mag.* **43** 153
[10] Jarrell M, Gubernatis J E and Silver R N 1991 *Phys. Rev.* B **44** 5347
[11] Silver R N, Gubernatis J E, Jarrell M and Sivia D S 1990 *Phys. Rev. Lett.* **65** 496
[12] Jarrell M, Gubernatis J E, Silver R N and Sivia D S 1991 *Phys. Rev.* B **43** 1206
[13] Bickers N E, Cox D L and Wilkins J W 1987 *Phys. Rev.* B **36** 2036
[14] Qin Q and Keiter H 1991 *Z. Phys.* B **84** 89
[15] Müller–Hartmann E 1984 *Z. Phys.* B **57** 281
[16] Keiter H 1976 *Z. Phys.* B **23** 37; Keiter H and Kurkijärvi J 1977 *Z. Phys.* B **26** 169
[17] Frota H O and Oliveira L N 1986 *Phys. Rev.* B **33** 7871
[18] Sakai O, Shimizu Y and Kasuya T 1989 *J. Phys. Soc. Japan* **58** 3666
[19] Sakai O, Shimizu Y and T. Kasuya 1990 *Physica* B **163** 695
[20] Costi T A and Hewson A C 1990 *Physica* B **163** 179; 1989 unpublished
[21] Costi T A and Hewson A C 1991 *Physica* C **185–189** 2649
[22] Costi T A and Hewson A C 1992 *J. Magn. Magn. Matter.* **108** 129
[23] Costi T A and Hewson A C 1992 *Phil. Mag.* B **65** 1165
[24] Costi T A and Hewson A C 1993 *J. Phys.: Cond. Matt. Lett.* **5** 361
[25] Costi T A, V. Zlatić V, Hewson A C and Coles B R 1994 *Physica* B **199** 81
[26] Zlatić V, Costi T A, Hewson A C and Coles B R 1993 *Phys. Rev. B* **48** 16152
[27] Zlatić V and Rivier N 1974 *J. Phys. F: Met. Phys.* **4** 732; Zlatić V and Horvatić B 1982 *J. Phys. F: Met. Phys.* **12** 3075

[28] Mahan G D 1981 *Many Particle Physics* (New York: Plenum) ch. 7
[29] Haldane F D M 1978 *Phys. Rev. Lett.* **40** 416
[30] Nozières P 1974 *J. Low Temp. Phys.* **17** 31
[31] Yamada K 1975 *Prog. Theor. Phys.* **53** 970
[32] Yamada K 1975 *Prog. Theor. Phys.* **54** 316
[33] Houghton A, Read N and Won H 1987 *Phys. Rev.* B **35** 5123
[34] Okiji A and Kawakami N 1983 *Phys. Rev. Lett.* **50** 1157
[35] Kawakami N, Usuki T & Okiji A 1987 *J. Phys. Soc. Japan* **56** 1539
[36] Hamann D R 1967 *Phys. Rev.* **158** 570
[37] Hewson A C 1993 *Phys. Rev. Lett.* **70** 4007; 1993 *J. Phys.: Condens. Matter* **5** 6277
[38] Costi T A and Hewson A C *The Dynamic Susceptibility of the Anderson Model*, unpublished.
[39] Coleman P, Anderson P W and Ramakrishnan T V 1985 *Phys. Rev. Lett.* **55** 414
[40] Fert A 1973 *J. Phys. F: Met. Phys.* **3** 2126
[41] Bauer E 1991 *Adv. Phys.* **40** 417; Lees M R, Coles B R, Bauer E and Pillmayr N 1990 *J. Phys.: Condens. Matter* **2** 6403; Bauer E, Gratz E, Pillmayr N, Häufer T, Lees M R, Gignoux D and Schmitt D 1990 *Physica* B **163** 375; Bauer E 1992 *J. Magn. Magn. Matter.* **108** 27
[42] Šokčević D, Zlatić V and Horvatić B 1989 *Phys. Rev.* B **39** 603

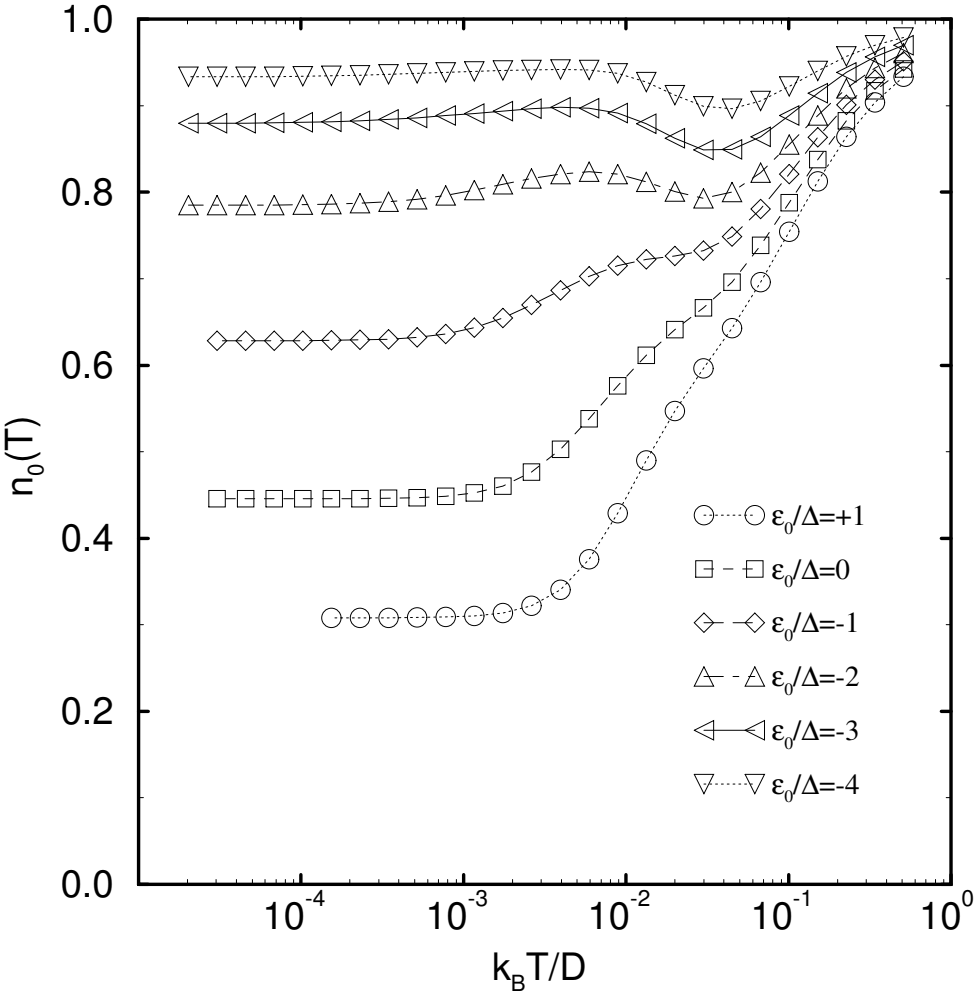

Figure 1. The local level ocuupancy $n_0(T)$ over the whole temperature range in various regimes.

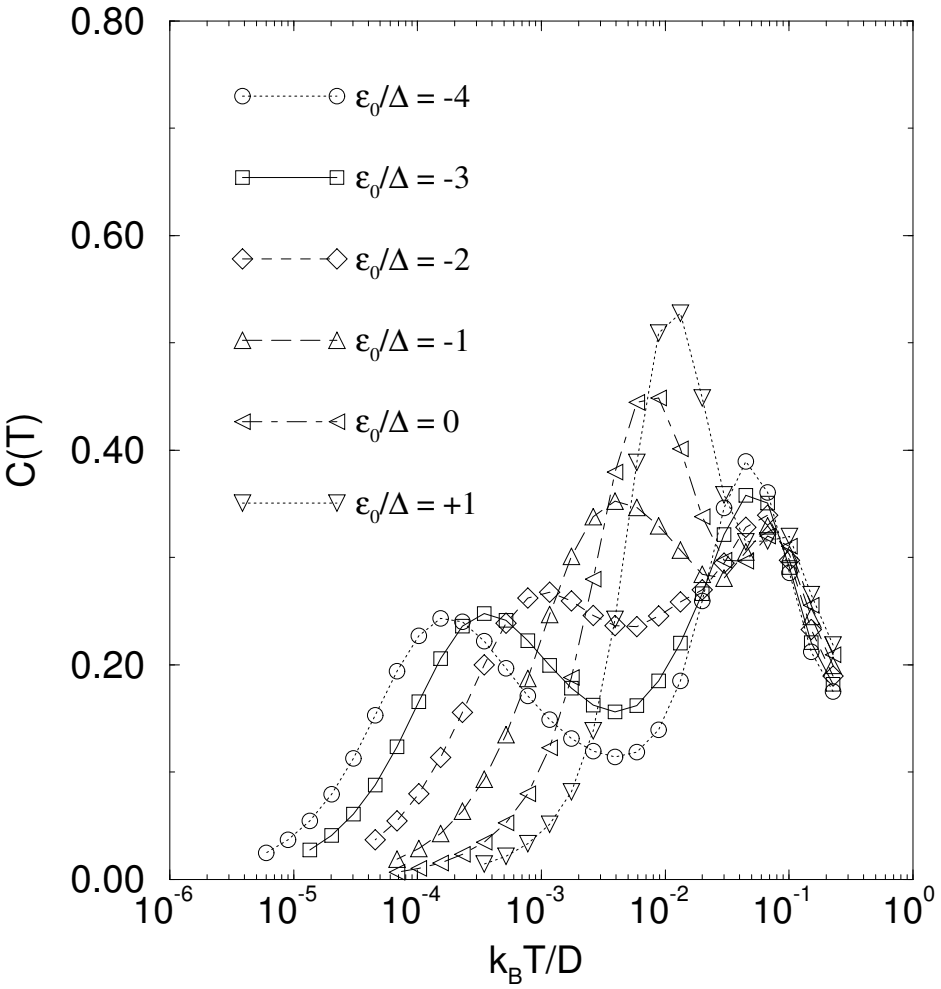

Figure 2. The specific heat in units of k_B over the whole temperature range and in the Kondo, mixed valency and empty orbital regimes.

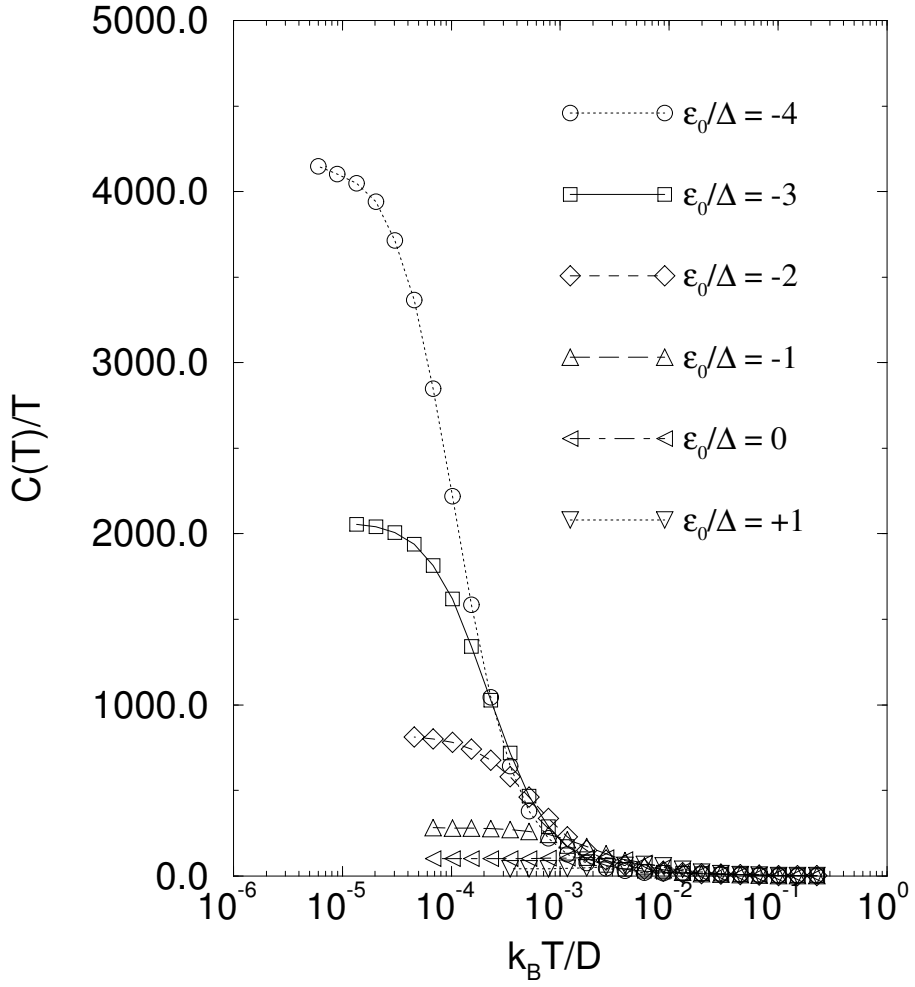

Figure 3. The specific heat exhibits Fermi liquid behaviour, $C(T) = \gamma T$, at low temperature, $T \ll T_{\rm K}$, in all parameter regimes. Note the very much enhanced values of γ in the Kondo cases compared to the mixed valency and empty orbital case.

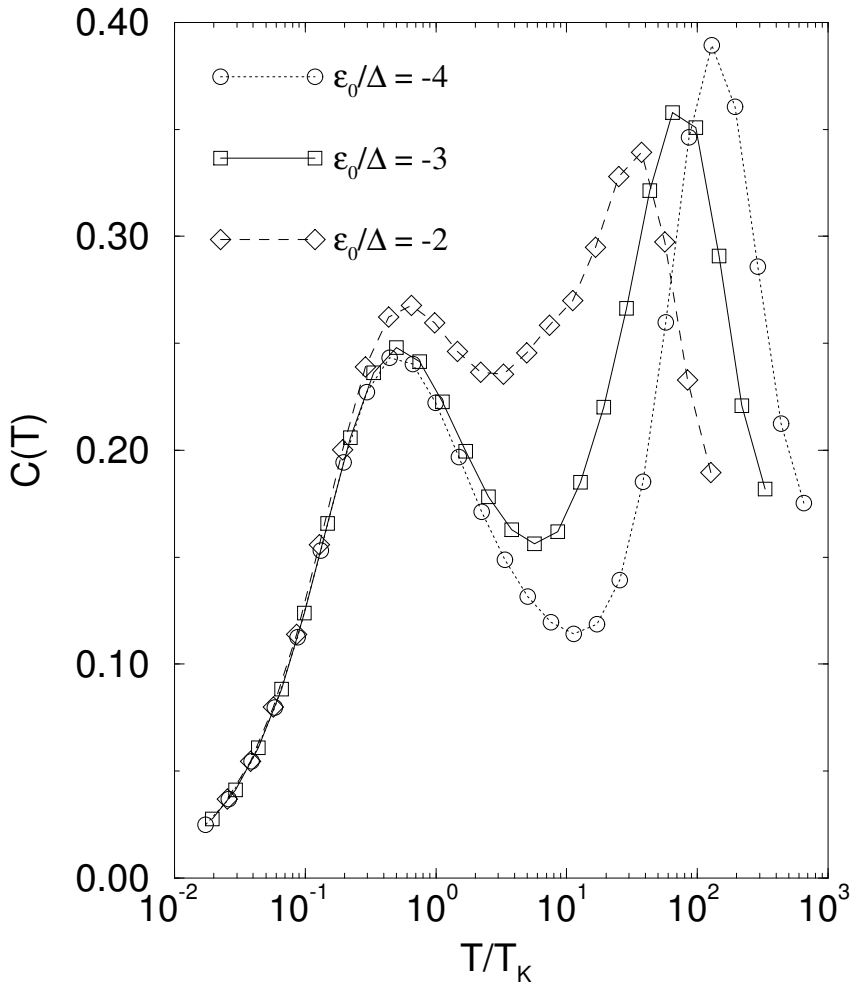

Figure 4. The specific heat in the Kondo regime, showing the universal behaviour for $T \leq T_{\rm K}$. However, when the local level position is well separated from the Fermi level, universality extends up to almost $10T_{\rm K}$ over almost the entire range of the low energy peak. The two disticnt energy scales, $T_{\rm K}$, governing the low energy peak and $\Delta \gg T_{\rm K}$ governing the high energy charge fluctuation peak are clearly evident.

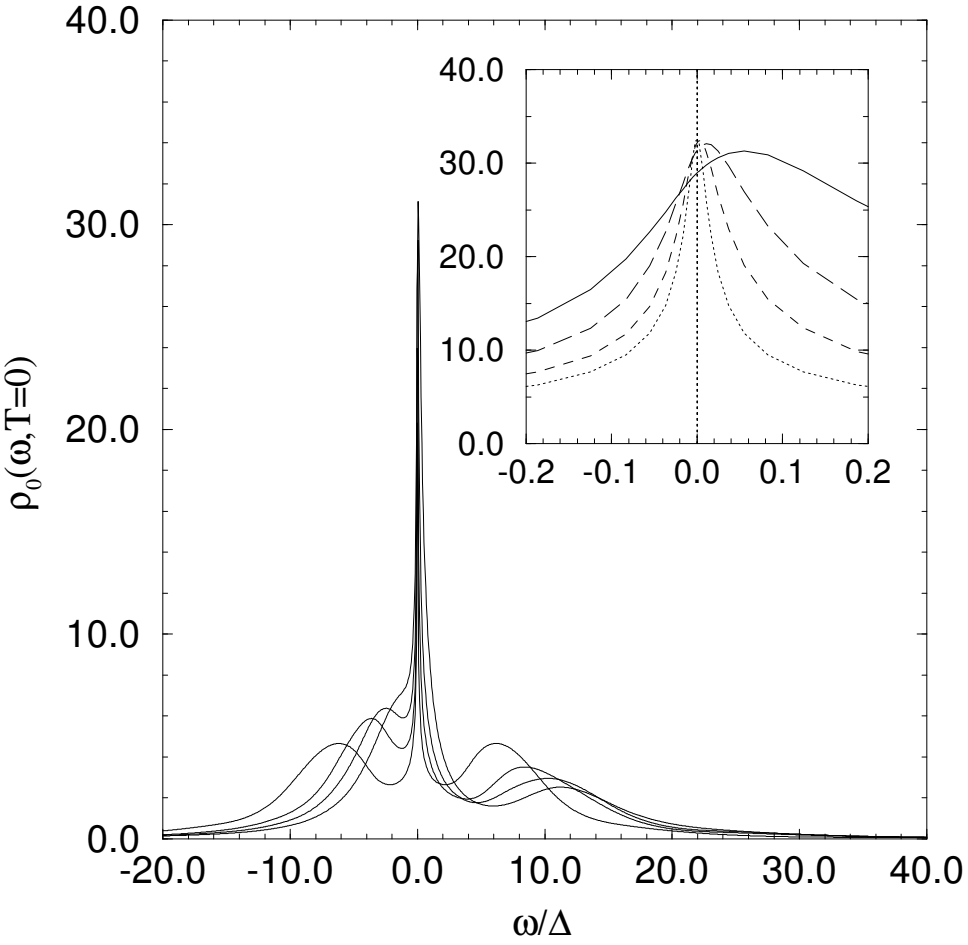

Figure 5. The $T = 0$ spectral density in the Kondo regime for several positions of the local level: the lower satellite peak is at the local level position ϵ_0. This takes values $\epsilon_0 = -U/2$ (symmetric case), $\epsilon_0/\Delta = -4, -3, -2$ (asymmetric cases). For $\epsilon_0/\Delta = -2$ the lower satellite peak forms a shoulder and has partly merged with the Kondo resonance. The high energy satellite peak is separated from the lower one by the Coulomb energy U. The inset shows the Kondo resonance in more detail. The Kondo resonance becomes broader as $-\epsilon_0$ decreases.

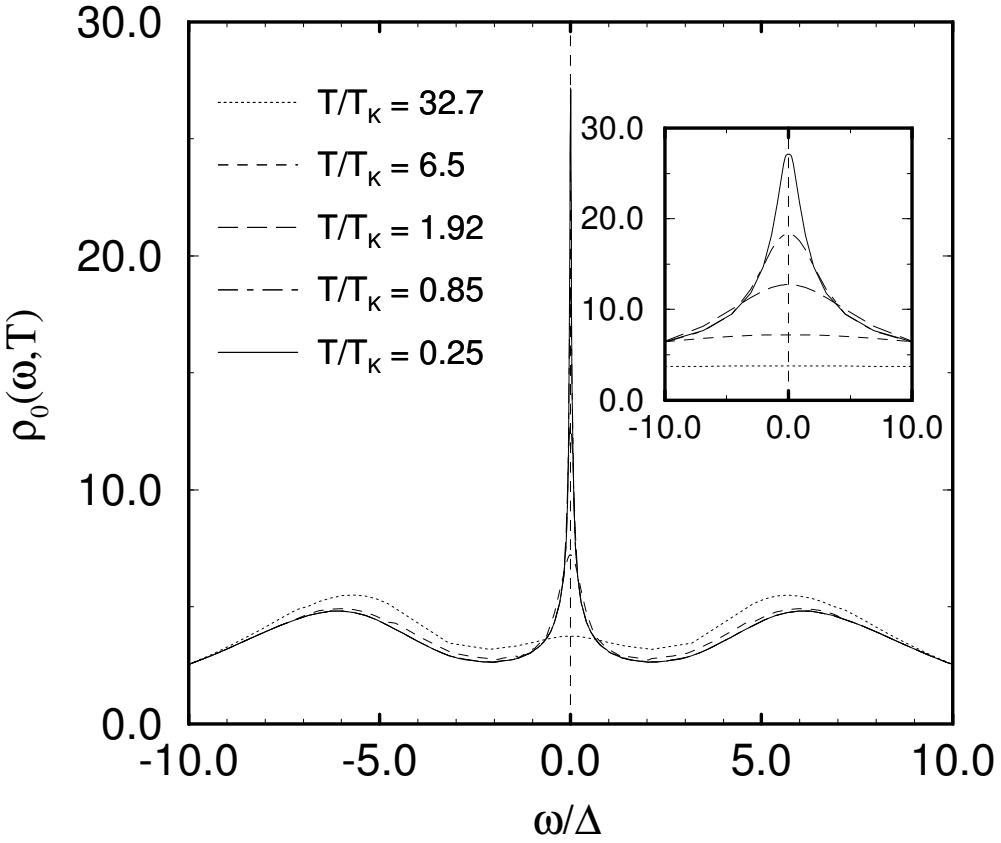

Figure 6. The finite temperature spectral density for the symmetric case. The inset is for $\rho(\omega, T)$ plotted versus $T/T_{\rm K}$ and shows in more detail the region around the Fermi level. The satellite peaks acquire some temperature dependence for $T \approx \Delta$.

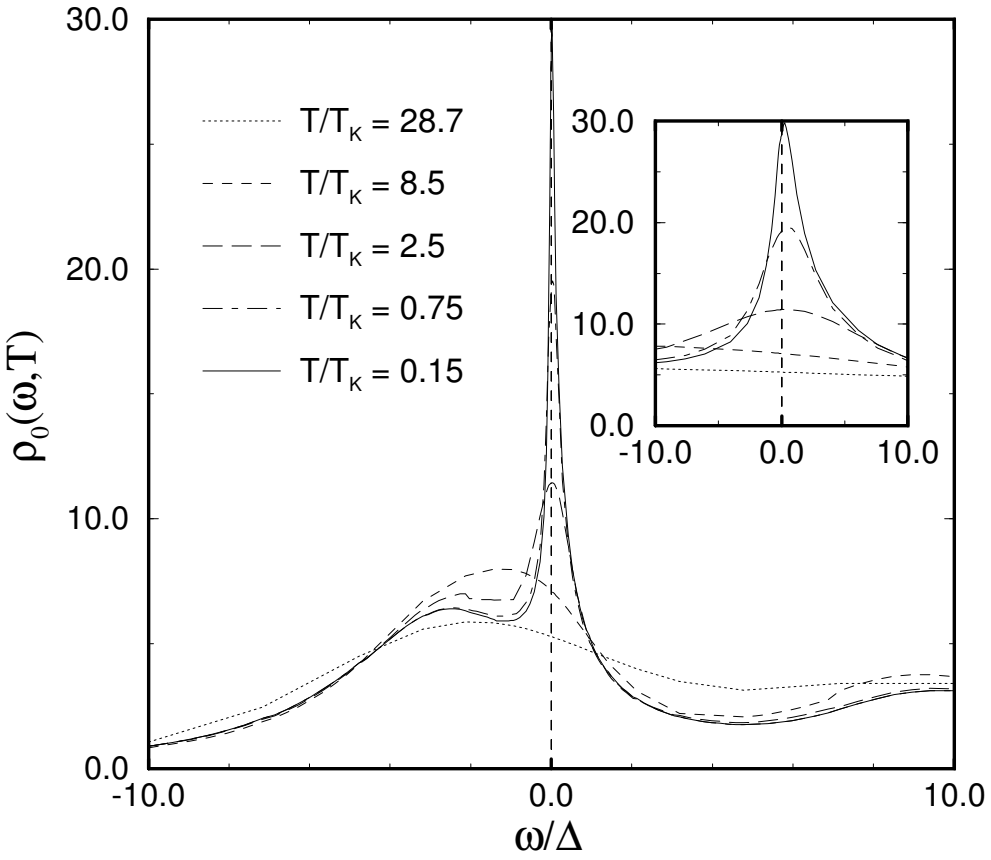

Figure 7. The spectral densities for the asymmetric case in the Kondo regime. At high temperatures $T \geq \Delta$ there is a shift of spectral weight from the lower to the upper satellite peak. The Kondo resonance, shown more clearly in the inset where it is plotted versus $T/T_{\rm K}$, disappears for $T \gg T_{\rm K}$.

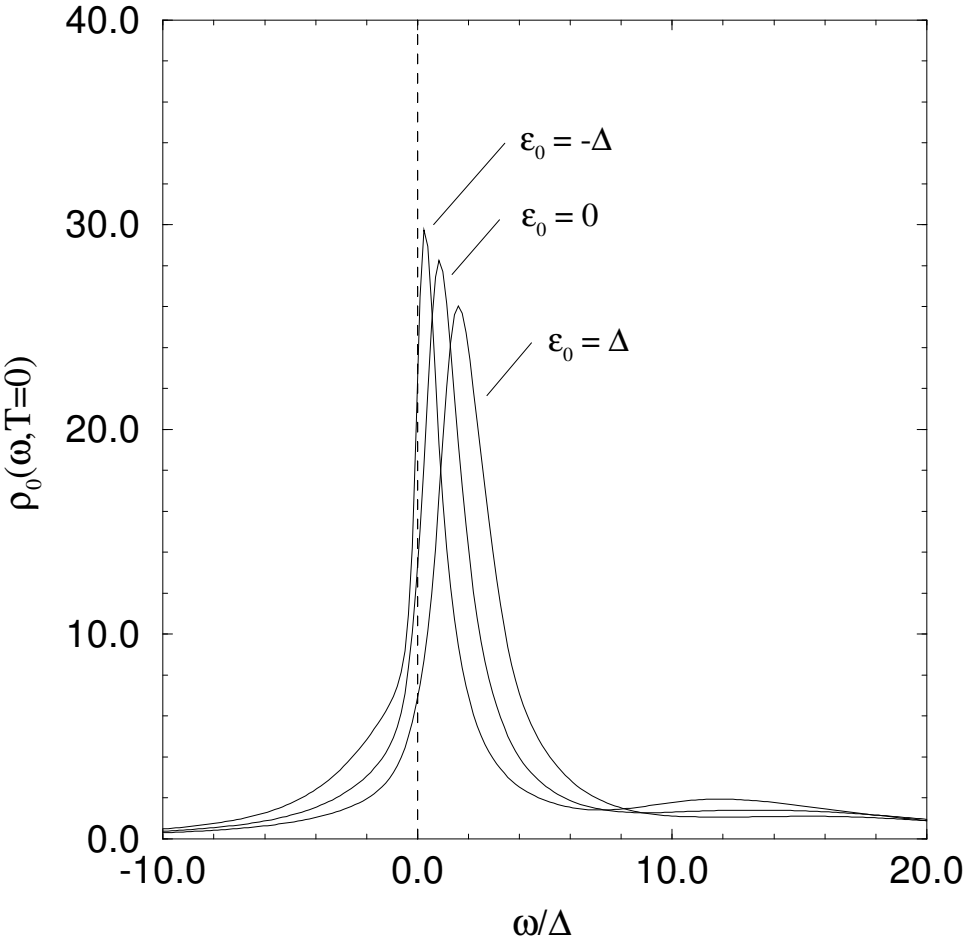

Figure 8. The $T = 0$ spectral densities in the mixed valency ($\epsilon_0/\Delta = -1, 0$) and empty orbital ($\epsilon_0/\Delta = +1$) regimes. The resonant level of width of order Δ is renormalized by the interactions to lie above the Fermi level. There is no Kondo resonance in these cases and the upper satellite peak at approximately $\epsilon_0 + U$ has very little weight.

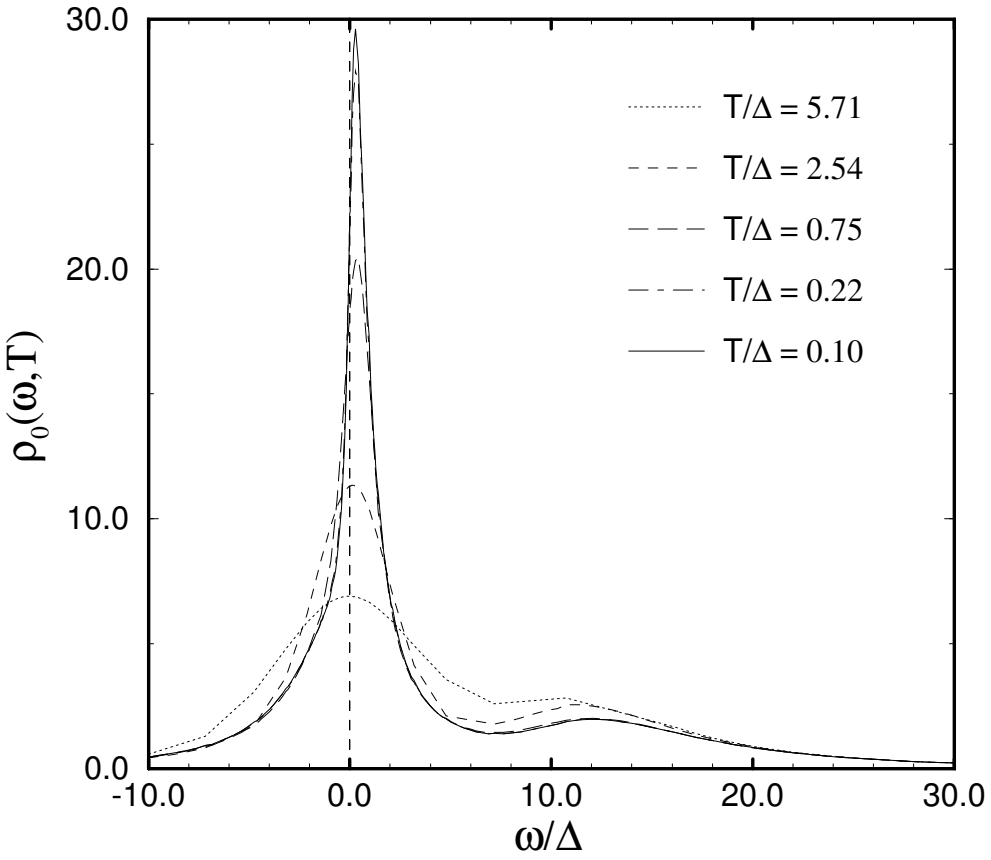

Figure 9. The temperature dependence of the spectral densities in the mixed valency regime. The renormalized resonant level of width Δ lying at $\tilde{\epsilon_0} > 0$ acquires a strong temperature dependence on a scale of $T \approx \Delta$.

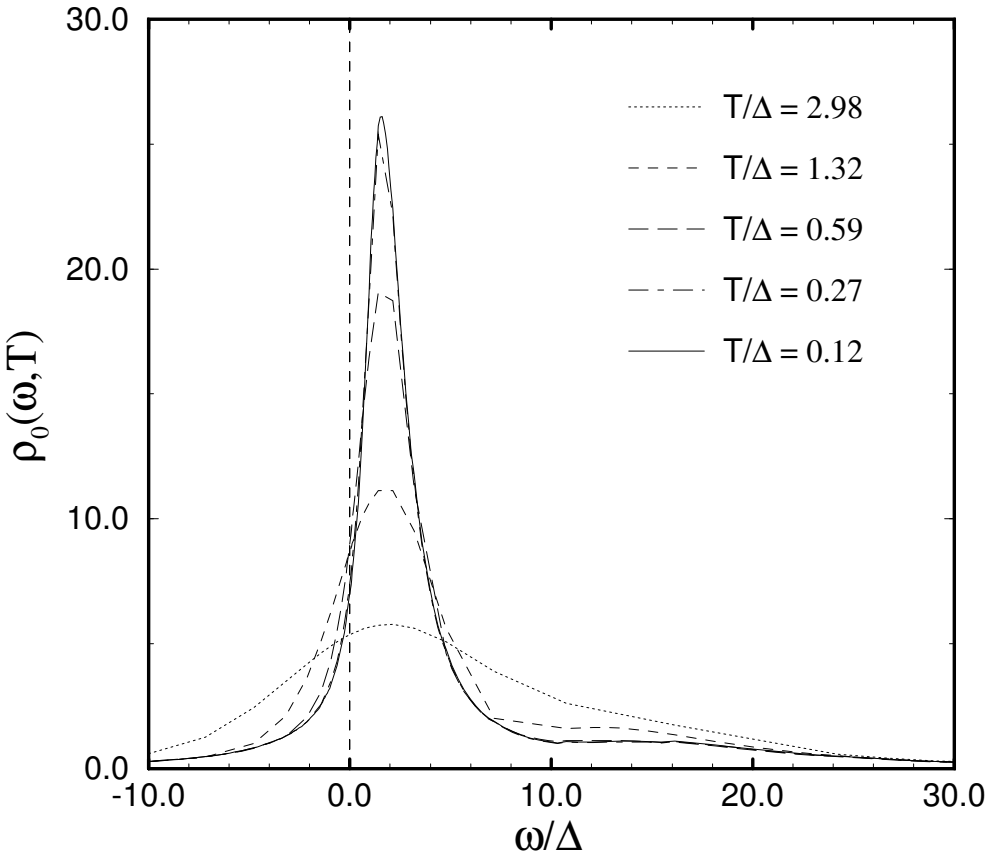

Figure 10. The temperature dependence of the spectral densities in the empty orbital regime. The relevant scale is the renormalized level $\tilde{\epsilon_0} > 0$ which for the present choice of parameters is approximately Δ. On a scale of $\tilde{\epsilon_0} \approx \Delta$ this resonance has a strong dependence on temperature.

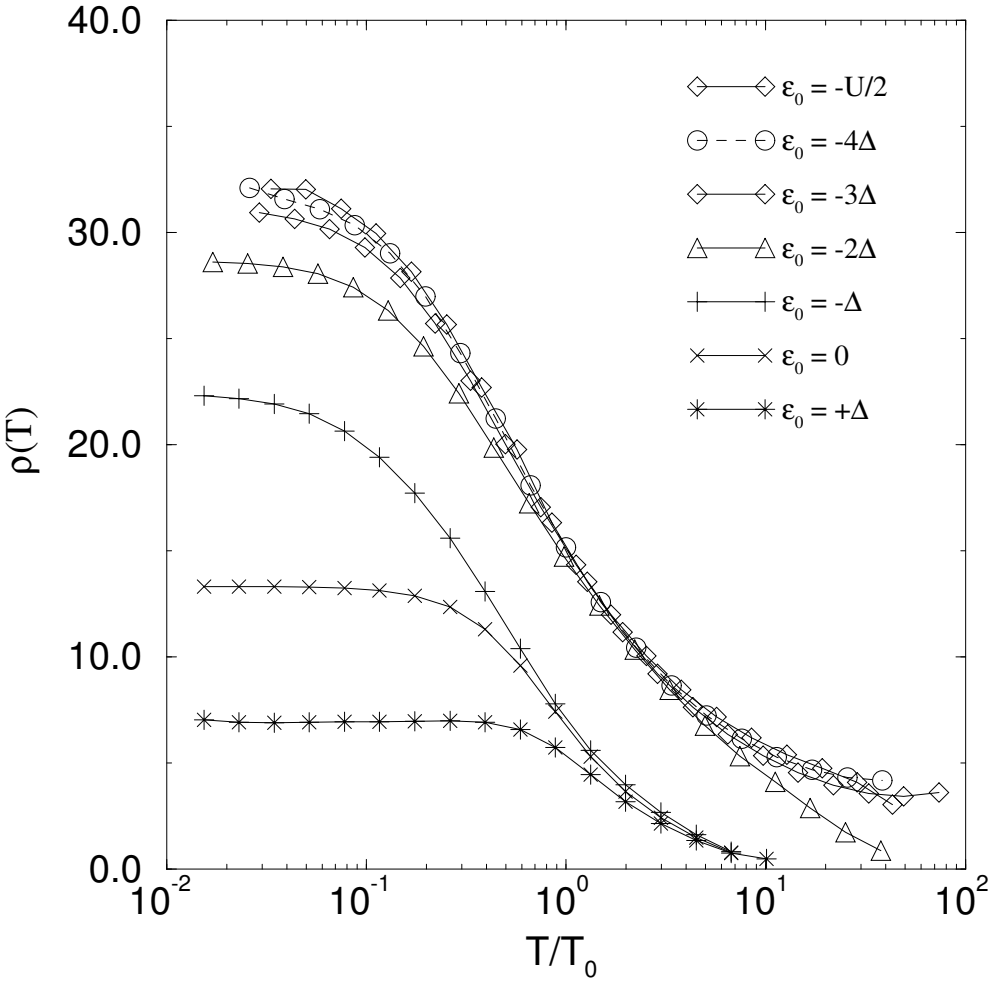

Figure 11. The electrical resistivity in various parameter regimes and over the whole temperature range. The curves are plotted versus the reduced temperature T/T_0, where $T_0 = \Delta$ in the mixed valency and empty orbital regimes and $T_0 = T_{\rm K}$ in the Kondo regime. The zero temperature value, $\rho(T = 0)$, is fixed by the Friedel sum rule to be $\sin^2(\pi n_0(T = 0)/2)/\pi\Delta$.

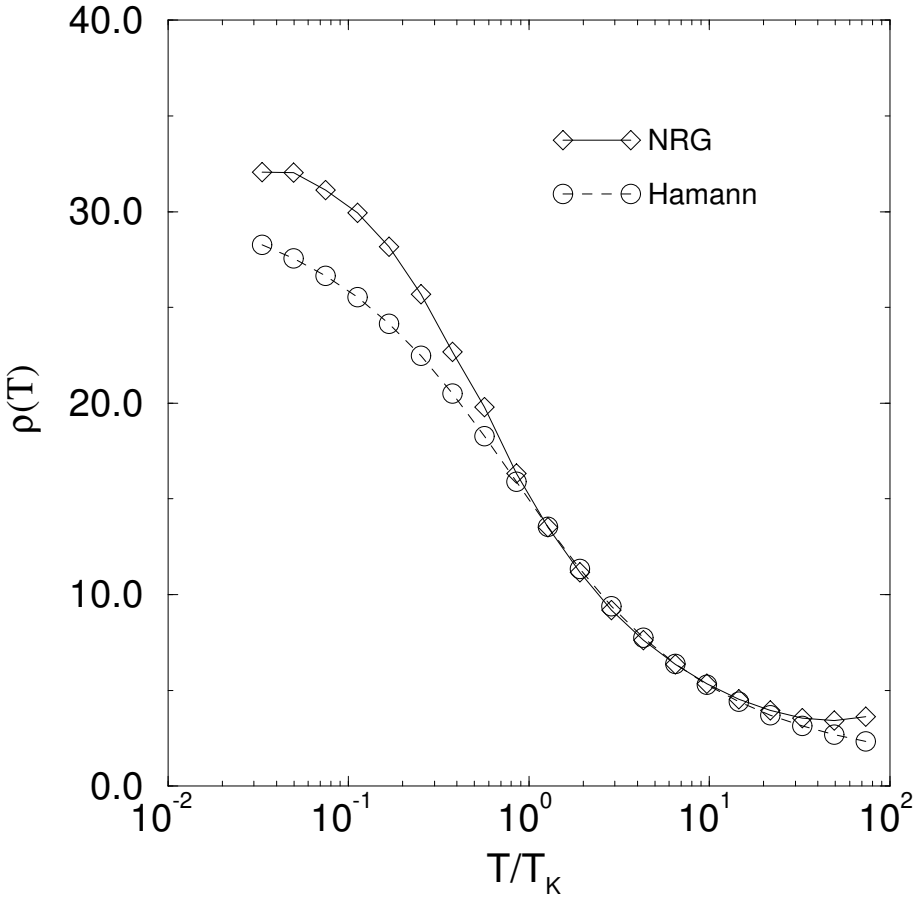

Figure 12. The resistivity in the symmetric case with a fit of the Hamann expression with $T_{\rm KH} = T_{\rm K}/1.2$. The Hamann result fits the high temperature range, and is very close to the NRG data for $T_{\rm K} \leq T \leq 10T_{\rm K}$. It fails at low and very high temperatures.

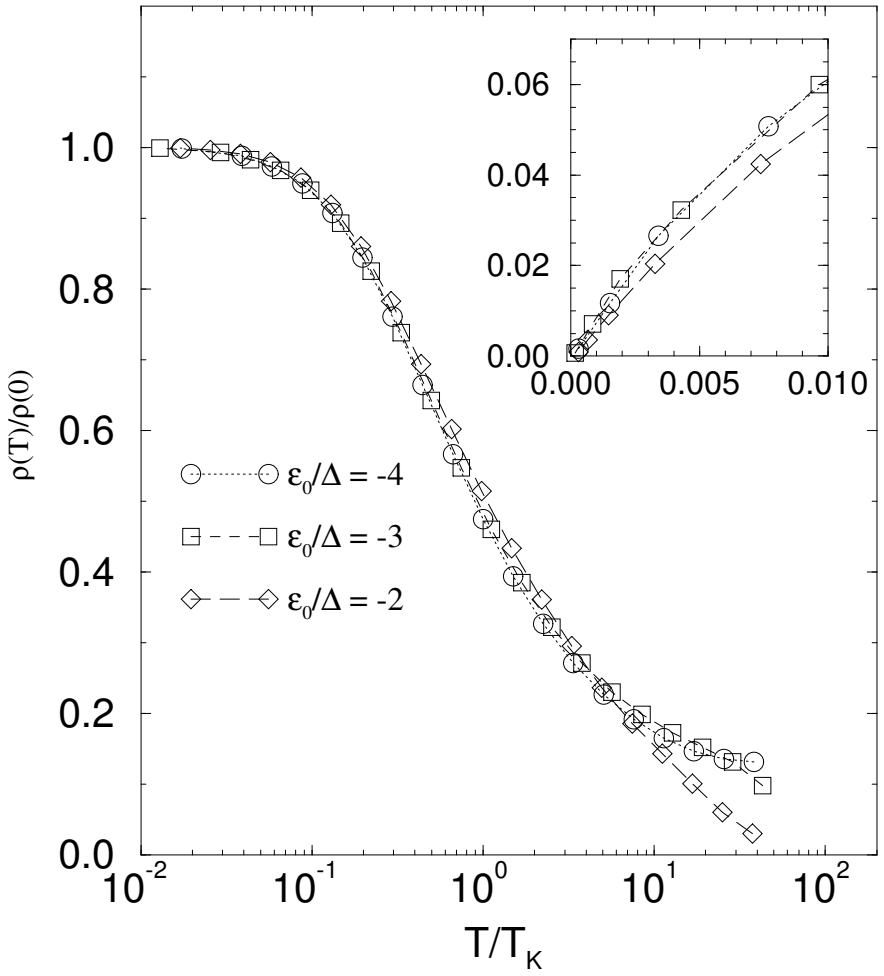

Figure 13. The scaled resistivity in the Kondo regime showing the universal behaviour at low temperature up to approximately $5T_{\rm K}$. The inset for $1-(\rho(T)/\rho(0))$ versus $(T/T_{\rm K})^2$ shows the expected Fermi liquid behaviour for the resistivity at low temperature $T < 0.1T_{\rm K}$. The coefficient, c, of the T^2 term in the resistivity is found to lie within 8 % of the exact result in all cases.

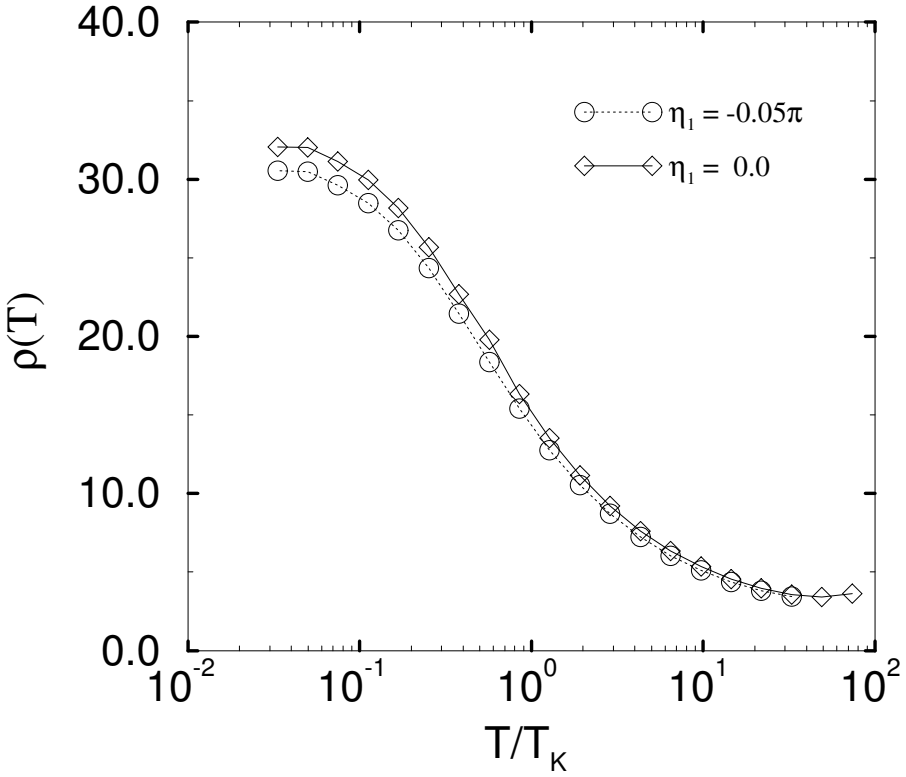

Figure 14. The influence of non–resonant scattering of conduction electrons on the resistivity in the symmetric Kondo regime.

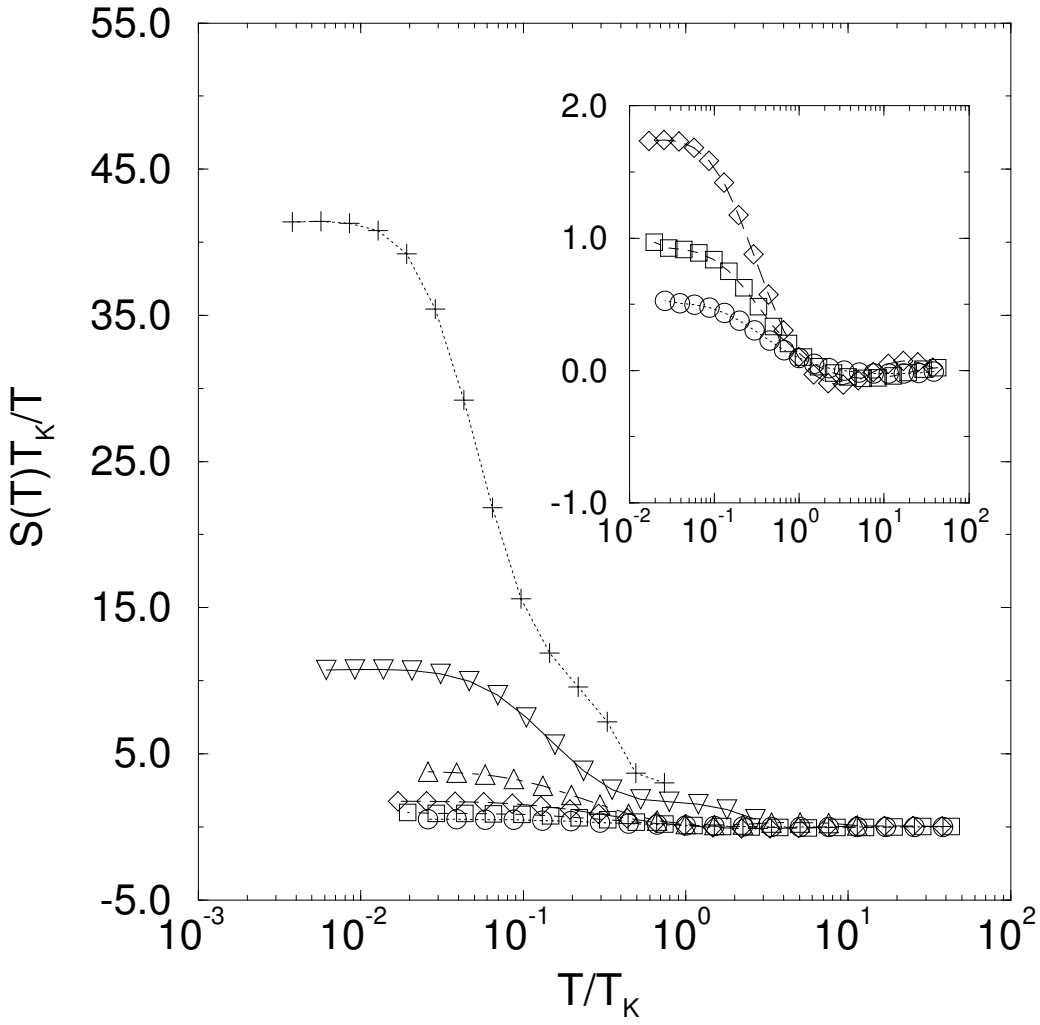

Figure 15. $S(T)/(T/T_{\rm K})$ showing the linear in T Fermi liquid behaviour of the thermopower for $T \ll T_{\rm K}$. The different curves are for local level positions $\epsilon_0 = -4\Delta(\circ)$, $\epsilon_0 = -3\Delta(\square)$, $\epsilon_0 = -2\Delta(\diamond)$, $\epsilon_0 = -1\Delta(\triangle)$, $\epsilon_0 = 0(\triangledown)$, $\epsilon_0 = +1\Delta(+)$. The inset shows the first three cases in more detail.

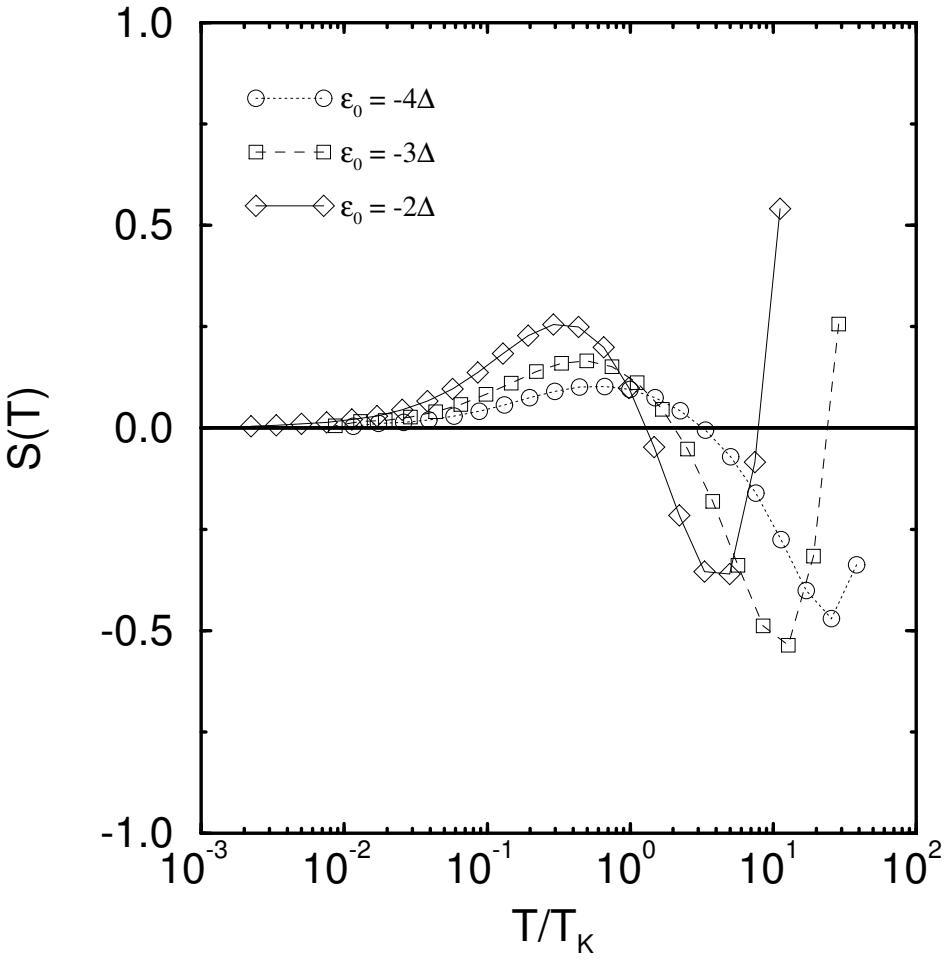

Figure 16. The thermopower $S(T)$ in the Kondo regime. The low energy maximum is at a temperature T in the range $T_{\rm K}/3 \leq T \leq T_{\rm K}$ whilst the broad minimum at higher temperature is at $T \approx \Delta$.

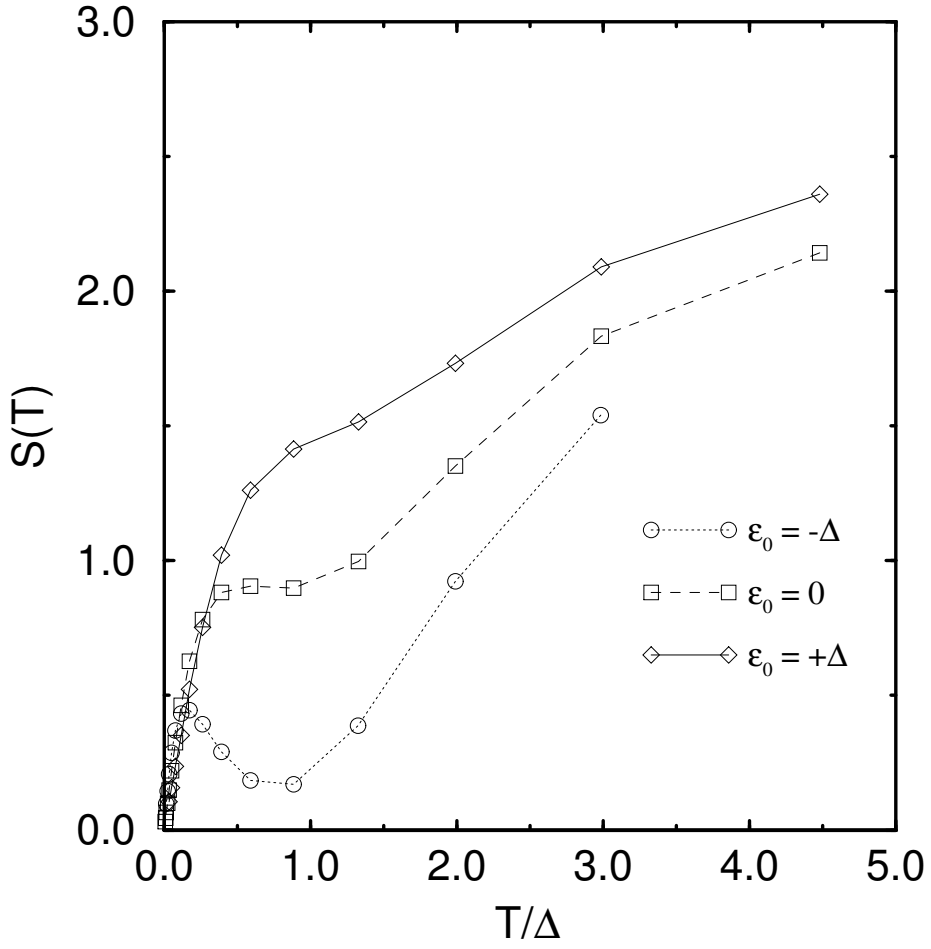

Figure 17. The thermopower $S(T)$ in the mixed valency and empty orbital regimes. The low energy maximum in the mixed valency case is in the range $\Delta/3 \leq T \leq \Delta$ and the minimum at higher temperature is at $T \approx \Delta$. In the empty orbital case, there is only a shoulder at $T \approx \Delta$

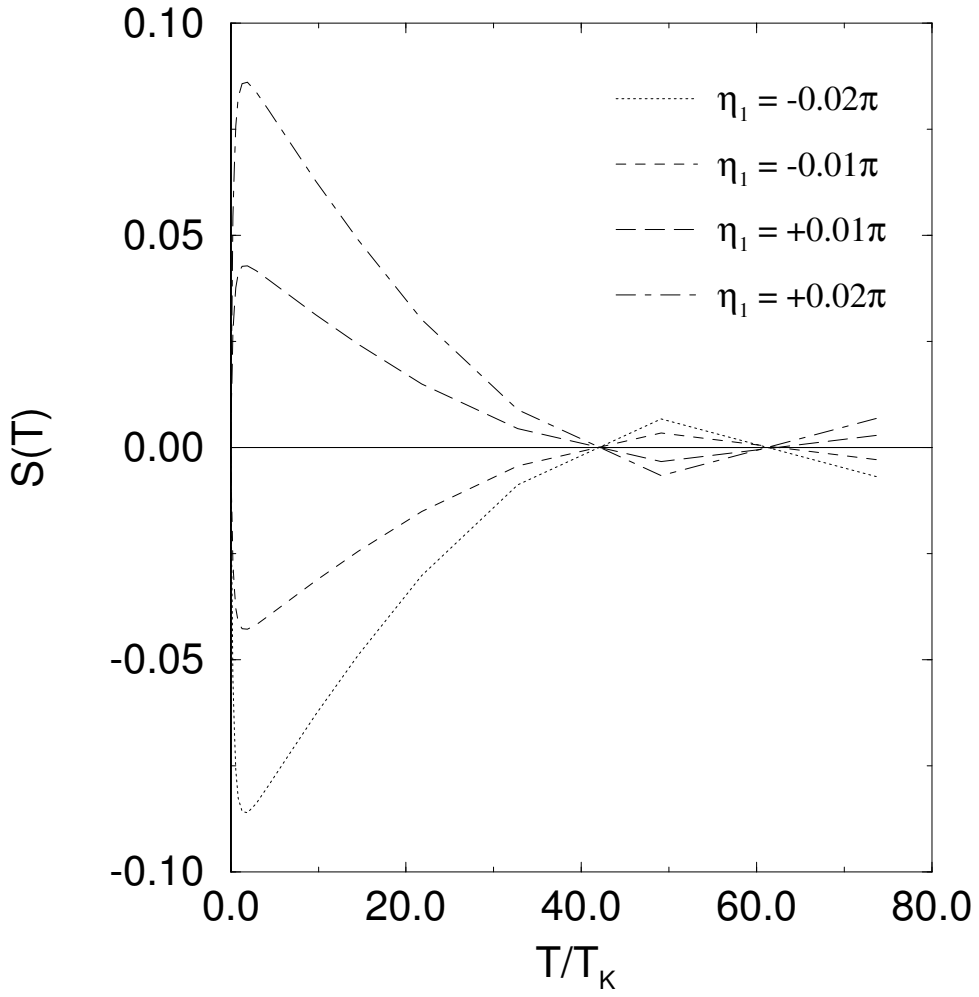

Figure 18. The thermopower $S(T)$ in the symmetric case with inclusion of non–resonant scattering. The low energy minimum is at $T \approx T_{\rm K}$ and the extremum at higher temperature is at $T \approx 50T_{\rm K} \approx 0.9\Delta$.

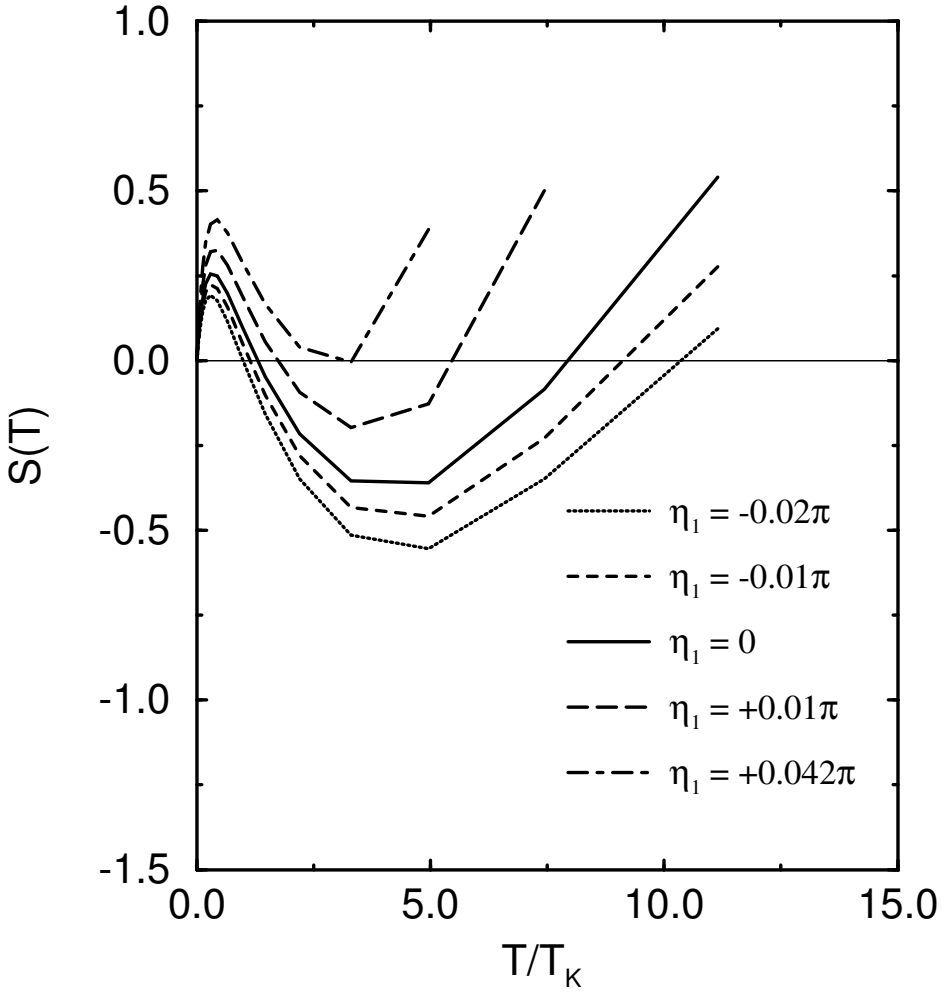

Figure 19. The effect of including non–resonant scattering on the thermopower in the Kondo regime $\epsilon_0 = -2\Delta$. For a large enough non–resonant phase shift $\eta_1 > 0.042\pi$ the broad minimum at $T \approx \Delta$ changes sign. The low energy maximum is at $T \approx T_{\rm K}/3$.

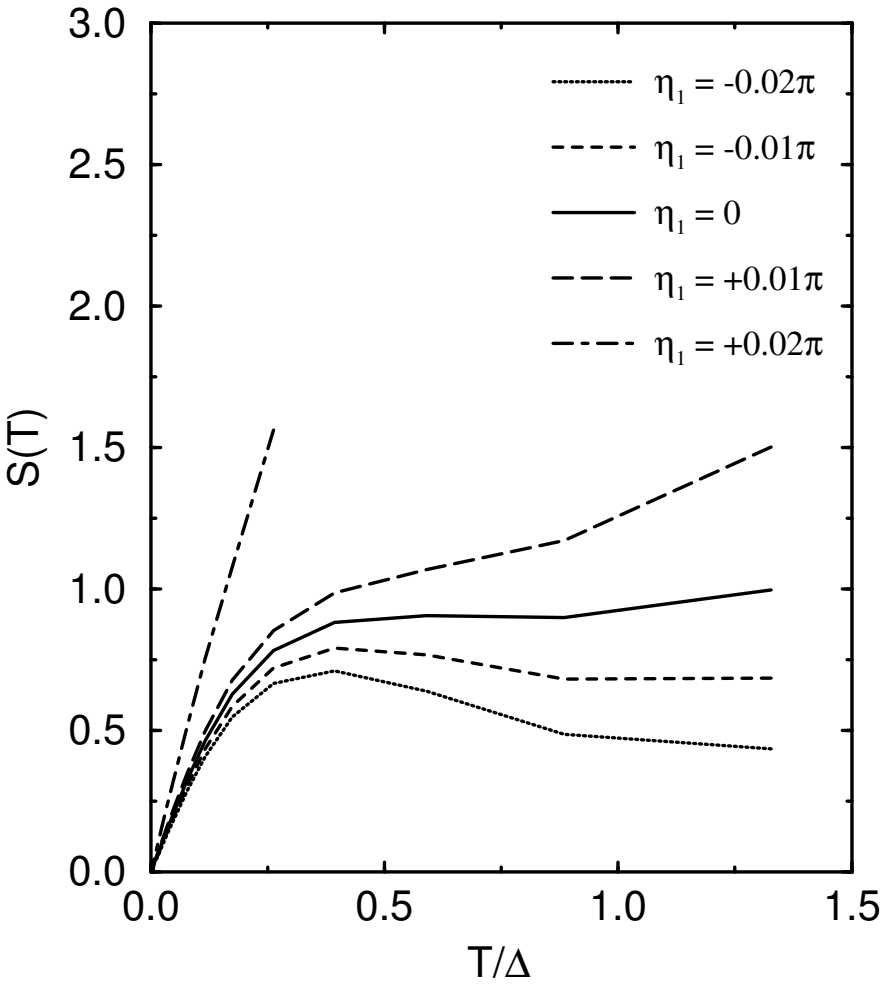

Figure 20. The effect of including non–resonant scattering on the thermopower $S(T)$ in the mixed valency regime $\epsilon_0 = 0$. There is only a broad maximum at $T \approx \Delta/3$ which disappears when the non–resonant phase–shift η_1 is increased.

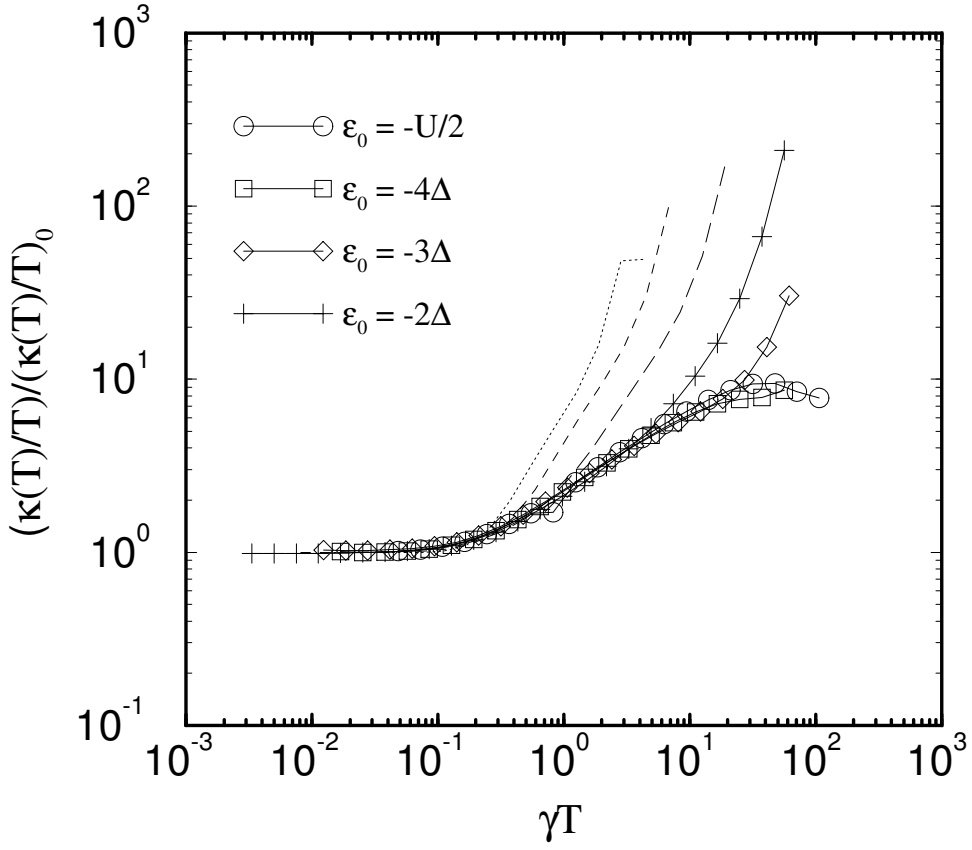

Figure 21. The thermal conductivity $\frac{(\kappa(T)/T)}{(\kappa(T)/T)_0}$ plotted versus $\gamma\, T$. The solid lines with symbols are for the Kondo regime. The mixed valency cases are $\epsilon_0 = -\Delta$ (long dashed) and $\epsilon_0 = 0$ (dashed), and $\epsilon_0 = -\Delta$ (dotted) is the empty orbital case. (The single point for the symmetric case which falls off the universal curve is due insufficient accuracy of the integrations at that particular temperature)

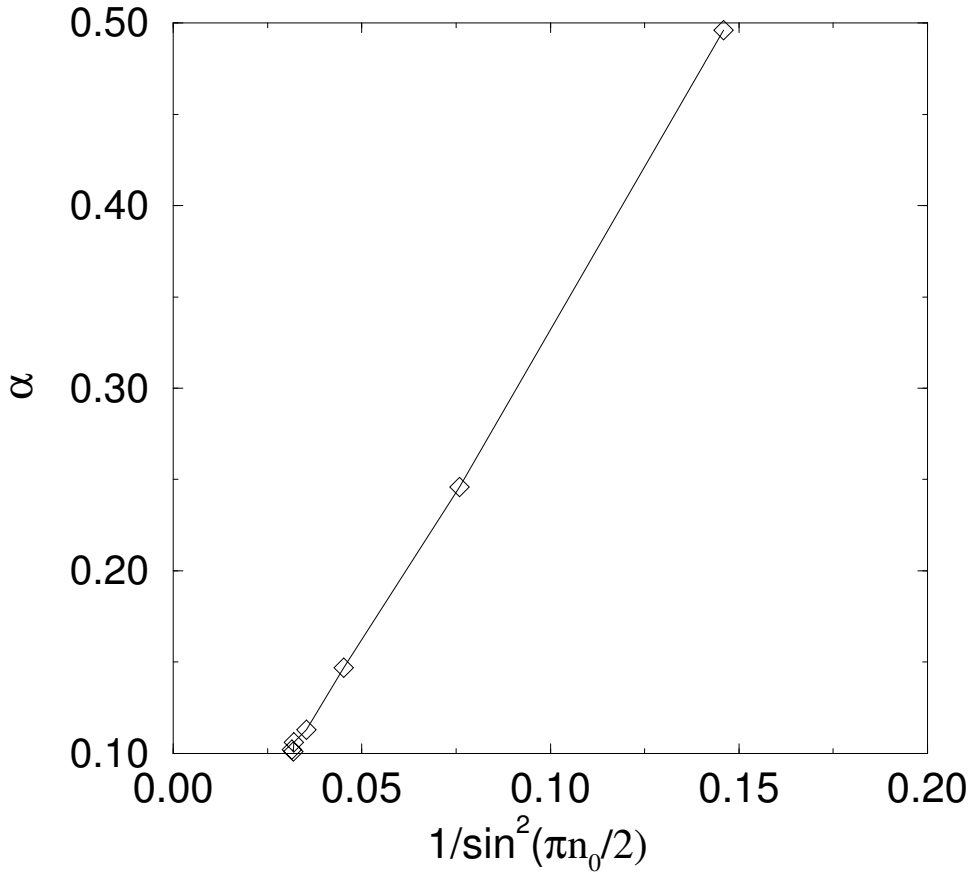

Figure 22. The linear coefficient of the thermal conductivity $\alpha = (\kappa(T)/T)_0$ versus $\frac{1}{\sin^2(\pi n_0/2)}$ (see Table I for the values).

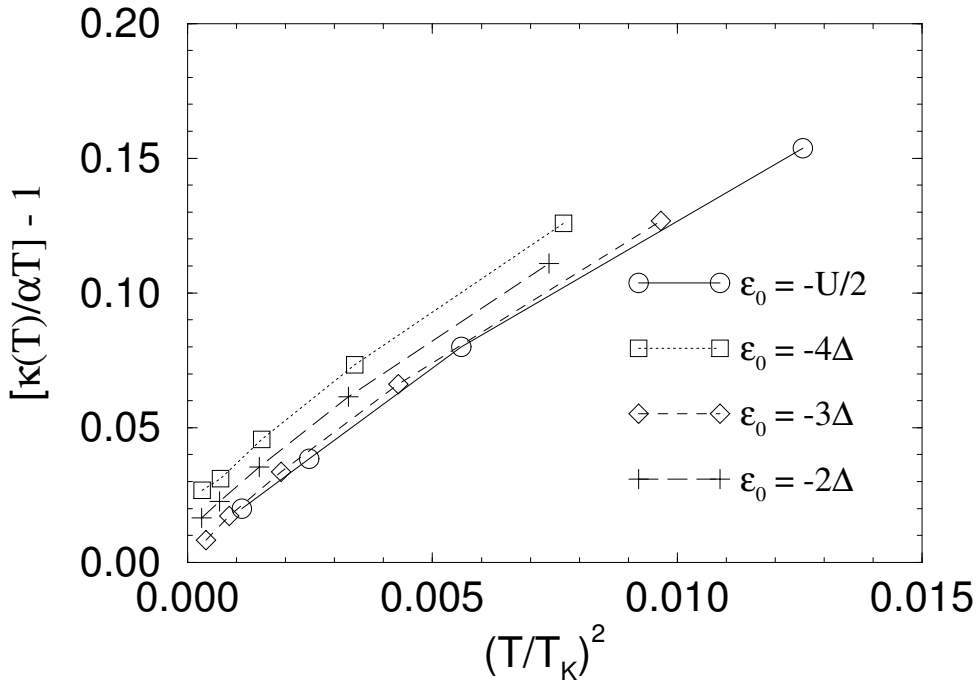

Figure 23. The T^2 coefficient of $\kappa(T)/\alpha T$ in the Kondo regime (see Table I for the values).

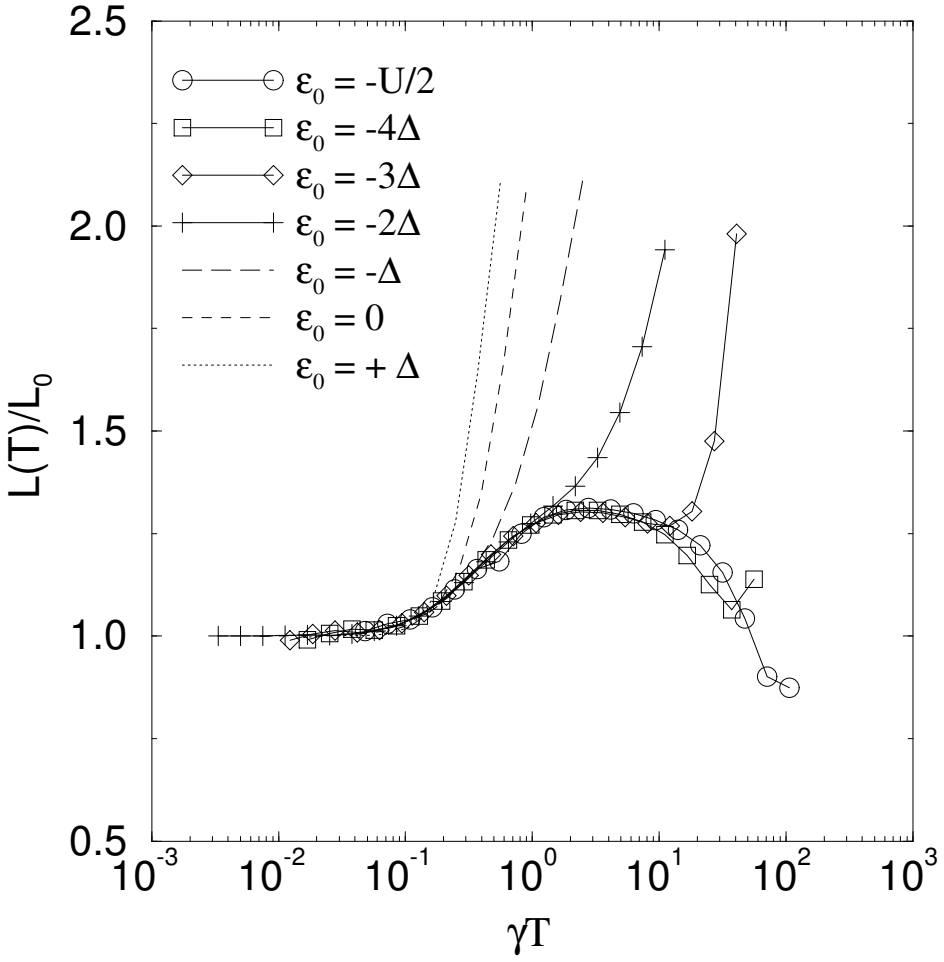

Figure 24. The Lorenz number ratio $L(T)/L_0$ where $L_0 = \pi^2 k_B/3e$ versus $\gamma\, T$.

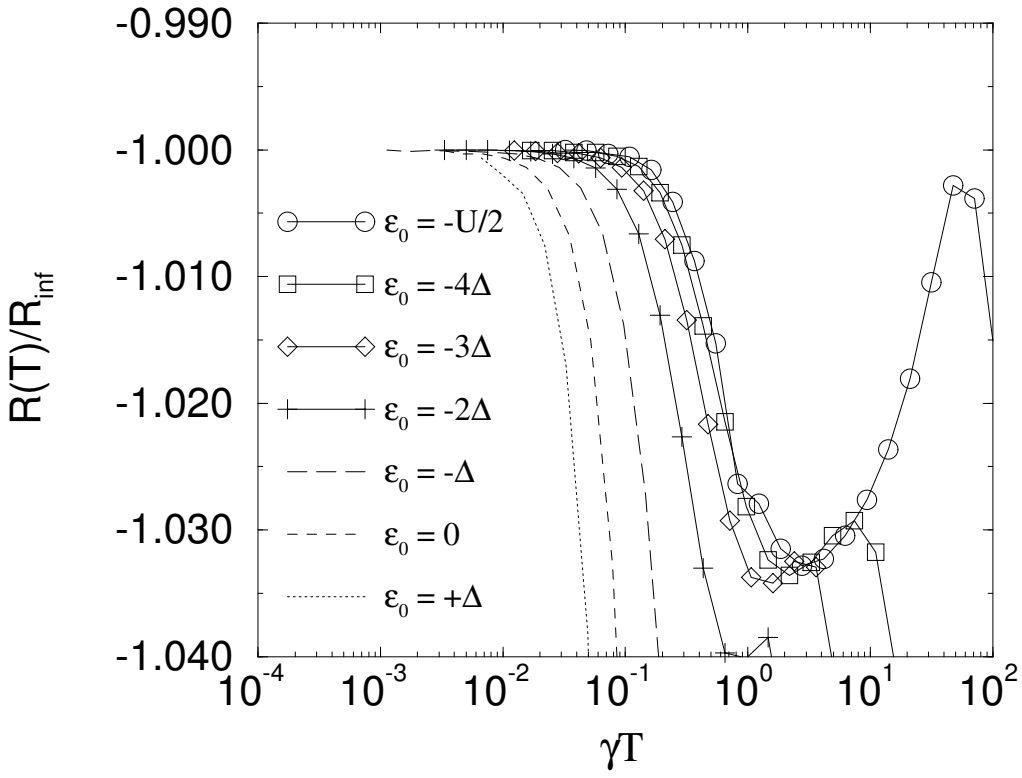

Figure 25. The Hall coefficient $R(T)/R_{inf}$ versus $\gamma\, T$ where $R_{inf} = -1/n|e|c$.

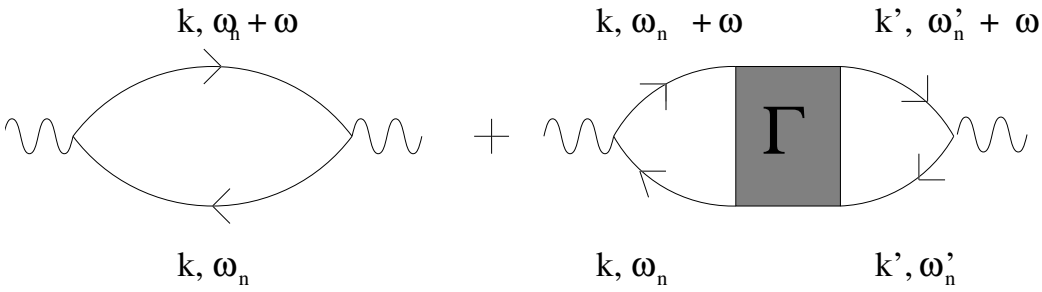

Figure 26. The diagrammatic representation of the current–current correlation function $\Pi(i\omega)$. The solid lines represent full conduction electron Green's functions and Γ is the two–particel scattering vertex.

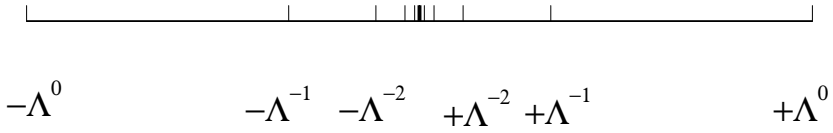

Figure 27. The conduction band $[-1, +1]$ logarithmically discretized with discretization parameter $\Lambda > 1$

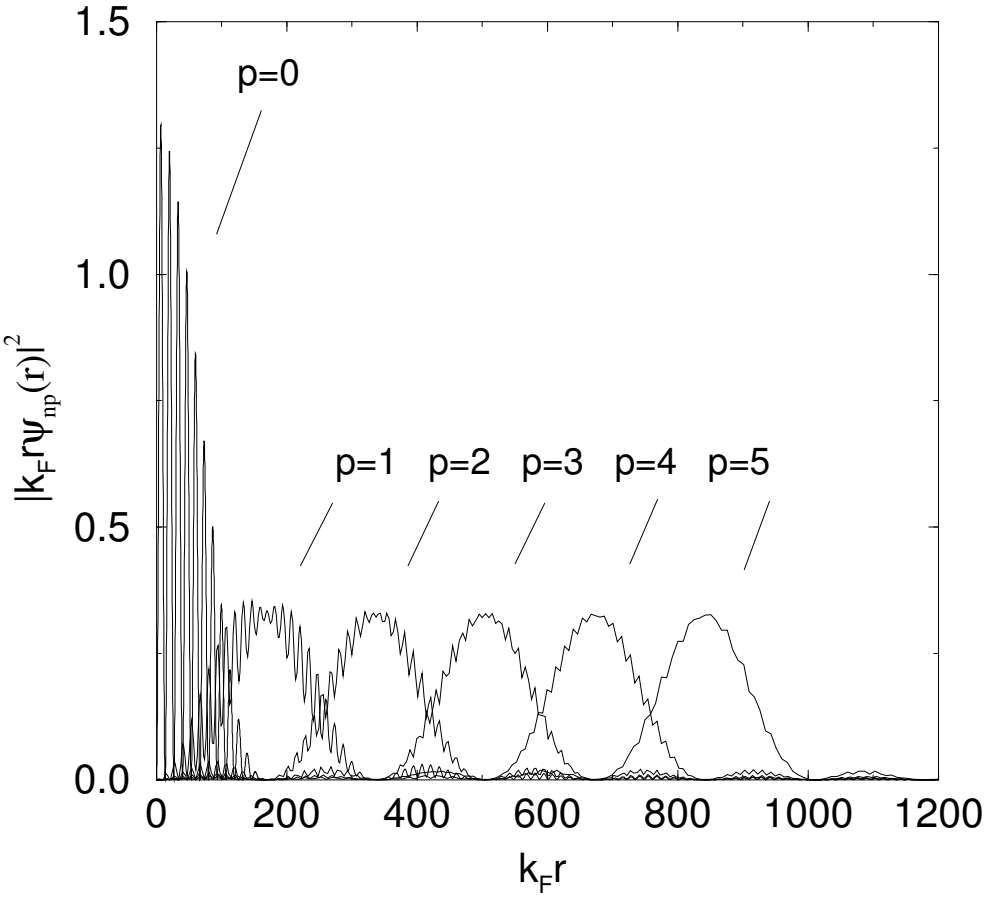

Figure 28. The normalized conduction electron orbitals $|k_F r\psi_{np}(r)|^2$ as a function of distance $k_F r$ from the impurity for $n = 5$ and $p = 0, 1, \ldots, 5$.